The Report Committee for James Kemper
Certifies that this is the approved version of the following Report:

Sensitivity analysis on Natural Fracture Properties and their Effect on Water Intrusion and Water Breakthrough Time in Fractured Reservoirs

APPROVED BY
SUPERVISING COMMITTEE:

Kamy Sepehrnoori, Supervisor

Wei Yu

Sensitivity Analysis on Natural Fracture Properties and their Effect on Water Intrusion and Water Breakthrough Time in Fractured Reservoirs

by

James Conner Kemper

Report

Presented to the Faculty of the Graduate School of

The University of Texas at Austin

in Partial Fulfillment

of the Requirements

for the Degree of

Master of Science in Engineering

The University of Texas at Austin

December 2020

Dedication

To my beautiful wife, who has lovingly supported me through it all, my warrior princess, Denver Rose, and my wild man, Jack.

Acknowledgements

I would like to express my sincerest thanks and deepest gratitude to my supervisor, Dr. Kamy Sepehrnoori for his support and encouragement during the past two years. Being a part of his group was such an incredible experience, and all of the learning, direction, and work ethic come from his leadership. It was such a profound experience getting to work alongside him and his group.

I am very grateful for and thankful to Mauricio Fiallos-Torres for his efforts and teaching over the past two years. He helped me in every detail of my research and I am incredibly indebted to him. If it were not for his help, and problem solving I would not have learned in the depth and understanding I did. I am very grateful for his time and teaching.

Sincerest thanks to Dr. Wei Yu for his guidance and support. He helped immensely in guiding my learning and research direction, and I am grateful to him for reviewing this report.

Additionally, I am appreciative of my colleagues in the research group for their teaching. So much of my learning stemmed from technical discussion and collaborative learning with them.

Finally, I am very thankful to my wife, family, and friends for their unconditional love and support through everything. These accomplishments pale in comparison to your greatness, and are a reflection of your trust and encouragement.

Abstract

Sensitivity Analysis on Natural Fracture Properties and their Effect on Water Intrusion and Water Breakthrough Time in Fractured Reservoirs

James Conner Kemper, MSE

The University of Texas at Austin, 2020

Supervisor: Kamy Sepehrnoori

Water intrusion can drastically impact production of hydrocarbons that hold the presence of an aquifer. This study analyzed how the presence of natural fractures, within a reservoir, can impact the timing and breadth of water intrusion. Natural fracture properties were varied in order to perform a sensitivity analysis as to what properties impacted water intrusion most heavily. The natural fracture properties that were varied over the course of this study were natural fracture density (number of natural fractures in a given reservoir volume), natural fracture conductivity, natural fracture length and aquifer properties. Three models were analyzed in this study: a tight reservoir model, a conventional carbonate reservoir model, and a dry gas field study. The tight reservoir model showed matrix permeabilities on the nano-scale, so fluid propagation was primarily driven through natural and hydraulic fractures. The tight reservoir model was used as a base case to better understand natural fracture properties' impact on water production, hydrocarbon production and producing ratio. No aquifer was present in the tight reservoir model. The conventional reservoir model had higher matrix permeabilities and porosities: however,

evident through the sensitivities, natural fractures with higher conductivity still governed fluid production in the conventional reservoir model. Statistical sensitivities on producing fluid ratios, water breakthrough time and producing fluids were run for each of these models. Differing aquifer models were run and compared for this study. The aquifer models used were the Fetkovich, and Carter-Tracy model using a commercial CMG modeling software. Water breakthrough time was determined by curvature changes analysis on the water production curve and confirmed using fracture saturation visualization in the embedded discrete facture modeling. Finally, a field study was conducted using the techniques and derived in the two conceptual cases (tight reservoir and carbonate reservoir). Analysis and sensitivities concluded that natural fracture number and natural fracture length had the most effect on water rate and hydrocarbon production.

Table of Contents

List of Tables

List of Figures

Chapter 1: Literature Review and Background

The basis of this report comes from a basic understanding of conventional and tight reservoirs, their fracture modeling, and different types of water drive and aquifer mechanisms. To understand these concepts, a literature review was conducted to better understand each on an appropriate level.

1.1 Fractured Reservoirs: Conventional and Unconventional

Conventional and unconventional reservoir exploration and production begins at the geologic and lithologic levels. *Figure 1*, below, shows these differences and highlights different reservoirs within each respective category (Burrows et al. 2020). This visualization highlights the inherent differences in pore size and permeability when being classified as conventional or unconventional. It is evident that the classifications of reservoir coincide with smaller pore sizes, and lower permeabilities (Burrows et al. 2020). Looking at the permeabilities, below 0.1 milli-Darcy (mD) of permeability are considered tight to extremely tight rocks and classified as unconventional. On the other hand, above this threshold are considered low to high permeability rocks and classified as conventional reservoirs. At the porosity level, nano to pico-pore sizes correspond to unconventional reservoir rocks while micro to macro-pore sizes correspond to more conventional reservoirs (Burrows et al. 2020).

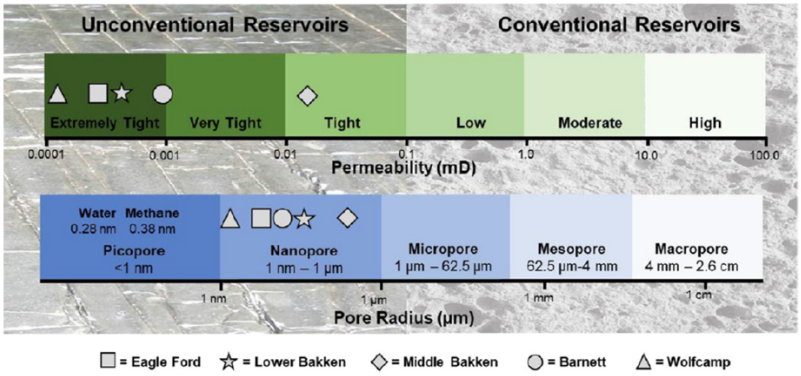

Figure 1: (Burrows et al. 2020) Comparison of permeabilities and pore radii in conventional and unconventional oil reservoirs. Permeability ranges from Canadian Society of Unconventional Resources. Pore size ranges from Loucks et al. 2012.

It is important to notice that the permeability ranges considerably by 3 orders of magnitude across the 5 fields listed– Eagle Ford, Lower Bakken, Middle Bakken, Barnett, and Wolfcamp. However, the porosity stays within 1 order of magnitude for all the reservoirs. Often the unconventional reservoirs are found in and produced from shalier type rocks. These reservoirs, along with lower permeability and porosity conventional reservoirs, often have large natural fracture networks throughout them (Burrows et al. 2020). This is due to the smaller grain sizes (silt to shale) and carbonate content. The smaller grain sizes, and chemical make-up create more fracture-prone rock. In turn, they are classified as “fractured reservoirs” and are an important focus of this study. For engineering purposes, it is important to understand how these natural fracture networks interact, and, in the subsurface, how their properties affect the flow of fluid throughout the reservoir.

1.2 FRACTURE MODELING

Over the years, and with the development of hydraulic fracturing and horizontal drilling technologies, these fracture modeling frameworks have grown as an area of focus for academia and industry knowledge. It began as early as 2002, with the growth of micro-seismic and temperature distribution sensors creating large data arrays indicating the complexity and size of the subsurface fracture networks created during hydraulic fracturing in horizontal wells (Maxwell et al. 2002; Fisher et al. 2004; Gale et al. 2007; Warpinski et al. 2008; Cipolla et al. 2010). These technologies indicated the importance of understanding how these fracture networks interact to understand the flow of fluids and their effect on production (Xu et al. 2017). This situation created a push for computational software designed to specifically model fractures. Many iterations of numerical frameworks and multiple approaches have been used over the years. Reservoir simulators have, since 1960, dual-porosity and dual-permeability models to model these fractures (Barenblatt et al. 1960; De Swaan 1976; Dean and Lo 1988). However, these type models are restrictive and unable to reproduce accurately complex fracture networks (Xu et al. 2017). Discrete fracture models (DFMs) were created and utilized the use of finite-difference and finite-element analysis to represent the complexity of the fracture networks more accurately. However, these DFMs are employed with unstructured grids which can be computationally expensive and even unrealistic for some field studies (Noorishad and Mehran 1982; Karimi-Fard and Firoozabadi 2003; Monteagudo and Firoozabadi 2004; Matthai et al. 2005; Hoteit and Firoozabadi 2006; Sandve et al. 2012; Hui et al. 2013).

1.3 EMBEDDED DISCRETE-FRACTURE MODELING (EDFM)

Embedded discrete-fracture modeling (EDFM) was created as a solution to model these highly complex subsurface systems, and highly expensive DFM methods (Lee et al.

2001; Li and Lee 2008; Hajibeygi et al. 2011). This technique continues modeling with the accuracy of DFMs but with higher computational efficiency. EDFM adds the fractures as additional blocks to structured grids (Xu et al. 2017). These fractures are indexed, using non-neighboring connections and allow for unique fracture properties for groups of fractures or individual fractures. Additionally, these fractures can take on any specific geometries and be modeled and simulated using commercial reservoir simulators (Moinfar et al. 2014; Panfili and Cominelli 2014; Cavalcante Filho et al. 2015). For this study, that allows for efficient and complex fracture modeling using commercial reservoir simulators.

The EDFM method adds fractures as additional grid-blocks using non-neighboring connections (NNC). There are three types of NNCs: connection between a fracture segment and the matrix, connection between the fracture segment within the same fracture, and connection between intersecting fracture segments (Xu et al. 2017). Mathmatically, these NNCs are formulated using the following equations. For a NNC between 2 cells of an individual fracture, the mass balance equation is given by

$$V_b \frac{\partial}{\partial t}(\phi N_i) - V_b \vec{\nabla} * \sum_{j=1}^{n_p} \frac{\bar{\bar{k}} k_{rj}}{\mu_j} \xi_j x_{ij} (\vec{\nabla} P_j - \gamma_j \vec{\nabla} D) - q_i - q_i^{NNC} = 0 \qquad (1)$$

where q_i^{NNC} is the molar rate of component i exchanged through NNCs and it is defined by

$$q_i^{NNC} = \sum_{m=1}^{n_{NNC}} A_m^{NNC} \sum_{j=1}^{n_p} \frac{\frac{k_m^{NNC} k_{rj}}{\mu_j} \xi_j x_{ij} [(P_j - \gamma_j D) - P_j - \gamma_j D)_m^{NNC}]}{d_m^{NNC}} \qquad (2)$$

And n_{NNC} is the number of NNCs for a grid block, and $P_j - \gamma_j D$ represents the flow potential at the neighboring cell (Moinfar et al. 2014). A^{NNC}, k^{NNC}, and d^{NNC} are the area, permeability and distance used to determine the transmissibility factor between each NNC pair (Moinfar et al. 2014). For NNC between matrix and fracture cells, the above equations remain the same; however, d_m^{NNC} is defined differently. It is defined as

$$d_m^{NNC} = \frac{\int x_n dv}{V} \quad (3)$$

where x_n, dv and V are the normal distance, the volume element, and the volume of the grid block, respectively (Li and Lee 2008; Hajibeygi 2011). Finally, for the NNC connection between intersecting fracture cells, the following approach is used.

$$\frac{k^{NNC}A^{NNC}}{d^{NNC}} = \frac{T_1 T_2}{T_1 + T_2} \quad (4)$$

$$T_1 = \frac{k_{f1}\omega_{f1}L_{int}}{d_{f1}} \ \ldots \ T_2 = \frac{k_{f2}\omega_{f2}L_{int}}{d_{f2}} \quad (5)$$

where L_{int} is the length of intersection line bounded in a grid block, and ω_f, k_f, and d_f are the fracture aperture, fracture permeability and average of the normal distances from the center of the fracture to the intersection line (Karimi-Fard et al. 2004; Moinfar et al. 2014). In effect, it is transforming a physical problem into a simpler computational problem. Figure 2 shows a visual of how this works (Xu et al. 2017).

The accuracy of the EDFM method has been compared to past methods of fracture modeling. Fine-grid explicit fractures are an accurate but computationally expensive way of modeling complex fractures (Moinfar et al. 2014). EDFM method's results were compared to a fine-grid explicit fractures to better understand the accuracy and sensitivity to grid size in the models. The results of this analysis are below in Figure 3. From this figure, and relevant to this specific example, at higher resolutions, there is convergence between the EDFM algorithm and the fine-grid explicit method (Moinfar et al. 2014).

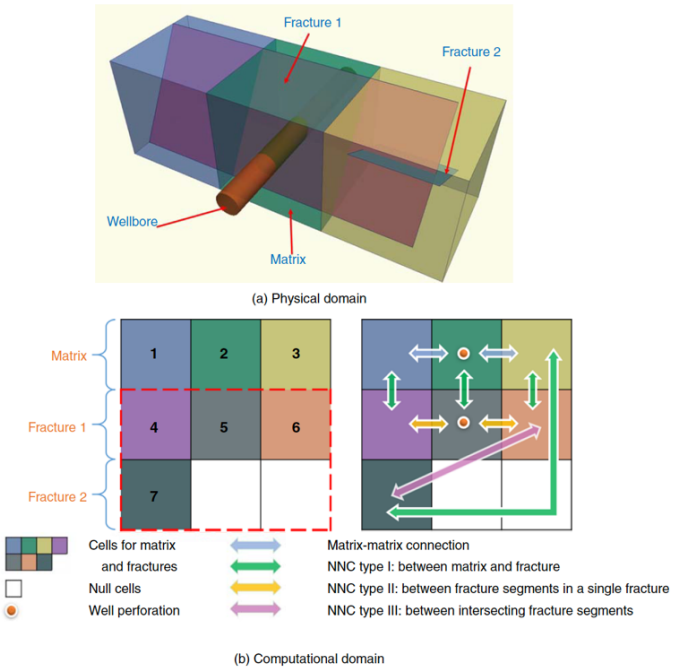

Figure 2: (Xu et al. 2017) Explanation of EDFM. In (a) the physical problem is defined - two fractures, 3 grid blocks, and the wellbore penetrating the matrix. In (b) this physical problem is transformed into a computation problem that can be efficiently simulated.

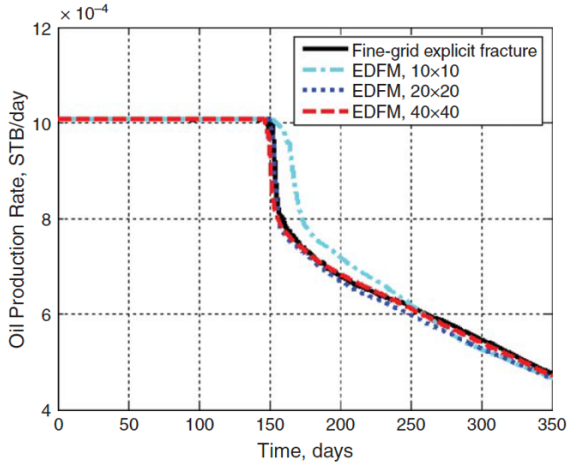

Figure 3: (Moinfar et al. 2014) Fine-grid explicit fracture model compared with EDFM with varying grid sizes.

Finally, a very popular method of defining and modeling fracture networks is the locally refined grid (LGR). This method can be very efficient, computationally speaking, for simple fracture geometries (Xu et al. 2017). However, when these fractures become more complex, local grid refinement can become more computationally expensive, and the EDFM method can outperform the LGR method in many scenarios. *Figure 4* shows a scenario presented in the paper by Xu et al. 2017. It shows a complex fracture geometry being modeled by LGR and EDFM methods. The two models' values are essentially equal (Xu et al. 2017). The computational time for the LGR and EDFM model, highlighted in *Figure 4*, was compared. The EDFM model, for this scenario and fracture geometry took 5% of the time that the LGR method took (Xu et al. 2017).

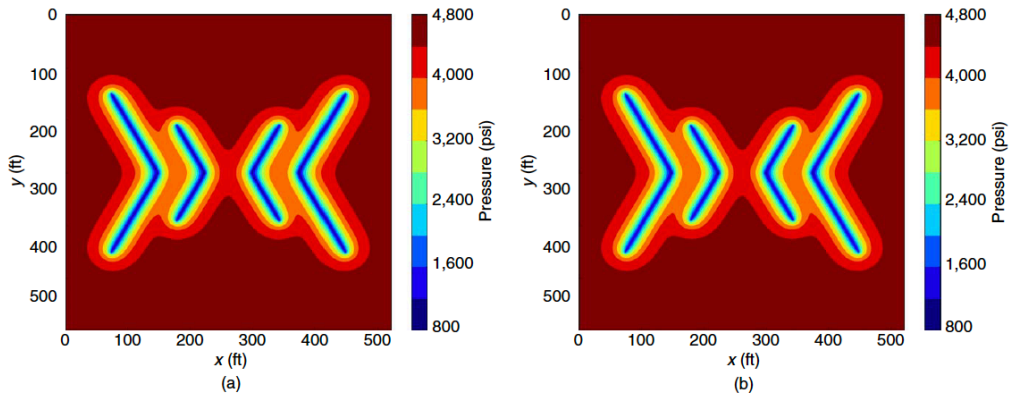

Figure 4: (Xu et al. 2017) Pressure comparison in a complex fracture using (a) LGR and (b) EDFM.

In conclusion, the EDFM method has been proven to be faster, and more accurate in modeling complex fractures and their networks. This was recognized in the literature review above by comparing to multiple methods of fracture modeling to the accuracy of the EDFM and the computational efficiency of the EDFM algorithm.

1.4 WATER INTRUSION

Water intrusion can drastically impact and negatively affect the production of hydrocarbons in naturally fractured reservoirs (Beattie et al. 1996; Inikori et al. 2002; Shen et al. 2015). The water intrusion can occur in many different ways: water coning, water fingering, and, for this study, channeling of water through highly conductive natural fractures (Chen et al. 2020). Once water has intruded into a fracture, it cuts off pathways for hydrocarbons to travel to the wellbore and can drastically reduce gas production. Additionally, naturally fractured reservoirs that sit on top of or adjacent to aquifers can be prone to early water intrusion and production (Chen et al. 2020). This is due to the highly permeable natural fractures cutting through the usually anisotropic rock ($\frac{k_v}{k_h} < 1$) and increasing the anisotropic permeability to the aquifer (Chen et al. 2020). This phenomena, once again, can reduce production of hydrocarbons as fractures are saturated with large amounts of water, effectively reducing the relative permeability of the hydrocarbons (Beattie et al. 1996; Inikori et al. 2002; Shen et al. 2015). Below, in *Figure 5*, is an example showing the water saturation in a couple fractures surrounding a well. This example has a strong aquifer positioned underneath the visible fractures. From the figure, it is clear that as these fractures are saturated with water over time, the hydrocarbon saturation is, effectively, reduced to its residual value. This water is then able to permeate through the fractures into the matrix and further create water coning and uneconomic water production.

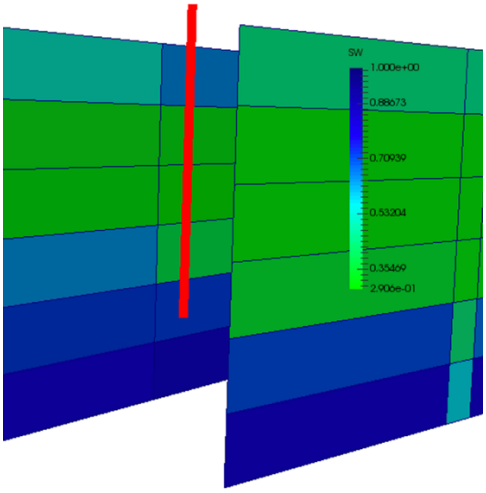

Figure 5: Schematic illustrating the drastic effect water intrusion into naturally fractured reservoirs can have on hydrocarbon production.

Since the fractures are highly permeable, in a naturally fractured reservoir, this schematic (Fig. 5) shows a keen example of how water intrusion, near the wellbore, can drastically reduce hydrocarbon production.

1.5 Aquifer Models

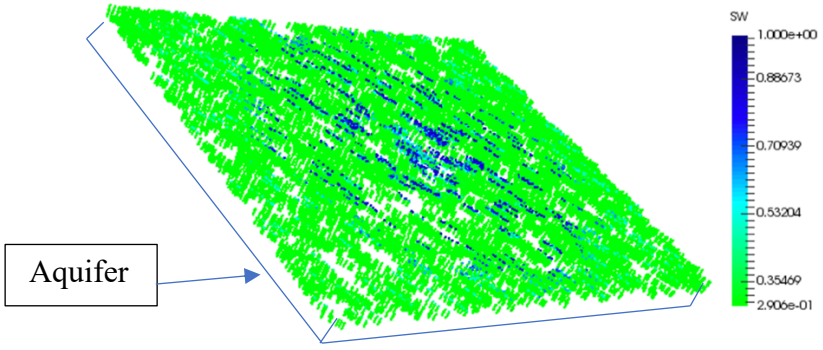

Figure 6: Visualization of the naturally fractured reservoir (green) and the aquifer sitting beneath it (wire frame).

The final background information needed for the completion of this study was the aquifer models. Two models were used, the Fetkovich model and the Carter-Tracy model. Both of these models are embedded in a commercial software that was used for this study. The software adds the aquifer, as a zero-thickness layer, in a posterior, anterior, or angled orientation to the reservoir. *Figure 6* shows an aquifer connected to the bottom of the reservoir. The properties of the reservoir – orientation, thickness, permeability, porosity, and radius – can be altered. The connection is still made as a zero-thickness grid, with different boundary conditions (Syed-Kechik and Hutchinson 1983).

M.J. Fetkovich outlined a simplified approach to water influx by assuming pseudosteady-state aquifer productivity index throughout the calculation. Originally, systems or reservoirs with the presence of an aquifer were broken into separate flow regimes – unsteady state, and steady state (Fetkovich 1971). This required either significant historical data, or core and geologic data when there was not enough historical production data on hand. Additionally, the historical data was needed in order to work through superposition in the calculations. His simplification eliminated the need for superposition in water drive models. It also created streamlined and standardized equations for a given boundary condition, flow regime, and flow geometry (Fetkovich 1971). He assumed that most flow geometries can be simplified, and, for engineering purposes, assumed to be either linear or radial (Fetkovich 1971). Those simplifications and corresponding equations are given in *Table 1*.

Finally, the Carter-Tracy model is also a simplification of previous water drive models, that eliminates the need for superposition in pressure and flow calculations (Carter-Tracy 1960). It is a simplification of the van Everdingen and Hurst models, which assume constant oil production rates (van Everdingen 1948; Hurst 1958). The Carter-Tracy method assumes constant water influx rates (Carter-Tracy 1960). In this method, the pressure

differential $[\Delta p(t_d)]$ is determined only from known quantities from the previous time step or tables of constants (*Equation 7*). This allows for more explicit determination of the pressure in each volume interval. Finally, these pressure values are inserted into the flow equation for water influx (*Equation 8*) for each time interval. As a consequence, this eliminates implicit trials and more efficient computation time in simulations (Carter-Tracy 1960).

$$\Delta p(t_{Dj}) = \frac{N_p(t_{D_j}) + W_p(t_{D_j}) - W_e(t_{D_{j-1}}) \left[\frac{P(t_{D_j}) - t_{D_j} P'(t_{D_j})}{P(t_{D_j}) - t_{D_{j-1}} P'(t_{D_j})} \right]}{B_0 \left[N c_e - N_p(t_{D_j}) c_0 \right] + B_1 \left[\frac{t_{D_j} - t_{D_{j-1}}}{P(t_{D_j}) - t_{D_{j-1}} P'(t_{D_j})} \right]} \quad . \quad . \quad . \quad (6)$$

$$W_e\left(t_{D_j}\right) = W_e\left(t_{D_{j-1}}\right) + \left(\frac{B_1 \Delta p(t_{D_j}) - W_e(t_{D_{j-1}}) P'(t_{D_j})}{P(t_{D_j}) - t_{D_{j-1}} P'(t_{D_j})} \right) (t_{D_j} - t_{D_{j-1}}) \quad . \quad (7)$$

where –

Δp: the change in pressure from $p(0) - \mathrm{p}(t_{D_j})$

W_e: cumulative water influx at current time-step

P: function defined at t_{Dj}

P': derivative of the function P

t_{D_j}: the present time-step

$t_{D_{j-1}}$: the previous time-step

B_1: a constant of proportionality defined by flow regime, porosity and compressibility of water and rock in the aquifer

c_e: composite compressibility of the oil reservoir

Type of Boundary	Radial Flow	Linear Flow
Finite – closed (no flow) at outer boundary	$q_w = \frac{7.08kh(\bar{p} - p_{wf})}{\mu\left[\ln\left(\frac{r_a}{r_r}\right) - \frac{3}{4}\right]}$	$q_w = \frac{3(1.127)kbh(\bar{p} - p_{wf})}{\mu L}$
Finite – constant pressure at outer boundary	$q_w = \frac{7.08kh(\bar{p} - p_{wf})}{\mu\left[\ln\left(\frac{r_a}{r_r}\right)\right]}$	$q_w = \frac{1.127kbh(\bar{p} - p_{wf})}{\mu L}$
Infinite	$q_w = \frac{7.08kh(\bar{p} - p_{wf})}{\mu\left[ln\sqrt{\frac{14.23kt}{\phi\mu c_t r_r^3}}\right]}$	$q_w = \frac{kbh(\bar{p} - p_{wf})}{\mu\sqrt{\frac{6.33kt}{\phi\mu c_t}}}$

Table 1: (Fetkovich 1971) Fetkovich equations for differing boundary conditions and flow geometries.

where –

q_w: water flow rate

$\bar{p}$: average aquifer pressure

p_{wf}: inner aquifer boundary pressure

μ: viscosity of the fluid

r_a and r_r: external radius of the aquifer, and internal radius of aquifer, respectively.

k: aquifer permeability

b: width in ft

h: height in ft

L: length in ft

ϕ: porosity

c_t: total or effective aquifer compressibility

t: time, days

Chapter 2: Conceptual Models

2.1 TIGHT RESERVOIR MODEL

2.1-1 The Grid Model

The original motivation for this analysis was to better study and understand water intrusion in various reservoir types and over an array of fractured reservoirs with differing permeability and petrophysical properties. Thus, a numerical model was used to better understand and analyze water intrusion in tight reservoirs. Additionally, several of the properties used in the sensitivity study, namely fracture permeability and fracture aperture, were combined in later studies to consolidate the sensitivity study. Figure 7 shows a visualization of the grid and wellbore after the model inputs. The grid size was 100x90x6. The size of each grid block was 50 ft in the x and y direction and 20 ft in the z direction – or 5000 ft x 4500 ft x 120 ft. The well in the model had a lateral length of 3828 ft. Moreover, there were 50 hydraulic fractures along the span of the horizontal. These hydraulic fracture properties were held constant for the study at 50 ft half-length and conductivity of 10 md/ft. They can be found in Table 2. This model did not include the presence of an aquifer. Instead, it was used as a baseline case to better understand the trends and sensitivities of natural fractures without the aquifer as an additional variable.

Hydraulic Fracture Parameter	Value	Units
Number of Fractures	50	
Fracture Half-Length	50	ft
Fracture Conductivity	10	md-ft

Table 2: Hydraulic Fracture parameters for the tight reservoir model

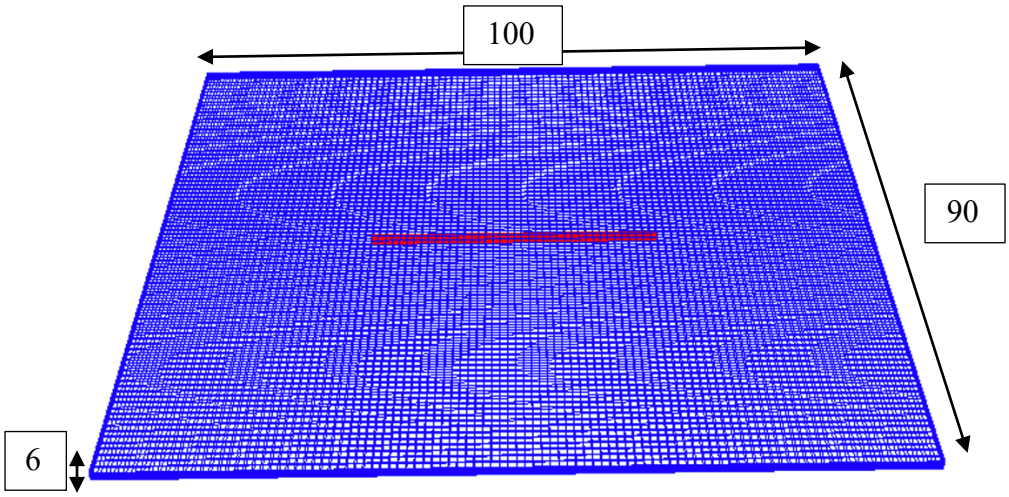

Figure 7: Visualization of the tight reservoir model grid and well formulation.

For the tight model, the matrix and reservoir properties used in this model can be found in *Table 3*.

Parameter	Value
Porosity, %	7.6-17.3
Permeability, nD	Matrix: 1-1000
Kv/Kh	0.1
Initial Water Saturation	0.3
Reservoir Pressure, psi	3696
Avg. Reservoir Thickness, ft (z)	120
Fracture Height, ft	120
Fracture Half-length, ft	50

Table 3: Table of matrix properties used for, and held constant, during the extent of the tight reservoir sensitivity analysis.

2.1-2 Fluid Model

For the conceptual model, a gas condensate model was used. A compositional model was chosen because gas condensates are better described using compositional

models rather than black oil models. The compositional models allow for more convenient recalibration of the different components when using PVT analysis (Izgec and Barrufet 2005). Additionally, the components were lumped into pseudo-components from lab report components. This allowed for more efficient simulation times, and kept accuracy while controlling macro parameters (API, volumetric factor, and GOR). *Table 4* contains the values of the fluid composition for this compositional model. It should be noted that these values were constant for both the tight and conventional conceptual model sensitivity studies.

Composition	
N2-CH4	0.7876
CO2-C2H	0.0936
C3H-IC5	0.08234
CO7-C11	0.0365

Table 4: Table containing the fluid composition for both the tight and conventional conceptual models used for the sensitivity studies

The values in *Table 3* and *Table 4* were constant for the duration of the analysis.

2.1-3 Sensitivity Analysis

The variables of change were the natural fracture properties found in *Table 5*. These values were varied by orders of magnitude, and cutoff values were determined where hydrocarbon and water production were no longer affected given higher or lower values of any given property.

For the analysis, natural fracture properties were varied by orders of magnitude given by the chart below. The dependent parameters used to measure the effect of the

variance of the parameters in *Table 5* were: water rate, cumulative oil, and cumulative water.

	Min	**Max**
Natural Fracture Permeability (mD)	0.01	1000
Natural Fracture Aperture (ft)	0.001	1
Number of Natural Fractures	1000	5000

Table 5: Table of ranges for the varying natural fracture parameters: fracture permeability, fracture aperture, and fracture density.

2.1-4 Results

Figures 8-19 show the results of the sensitivity study. The resulting variables were water rate (*Figure 8, 12, 16*), gas rate (*Figure 9, 13, 17*), cumulative gas production (*Figure 10, 14, 18*), and cumulative oil production (*Figure 11, 15, 19*). Varying parameters included fracture permeability, fracture aperture, and fracture density, and the effect on water rate and cumulative oil. The trend for each of these varying parameters is that as fracture conductivity is increased, water rate increases and cumulative oil decreases. The reason behind this result is that as fractures govern the flow of fluid in unconventional and tight reservoirs, increasing the transmissibility in these fractures would naturally increase the flow of fluid. As the natural fracture permeability and aperture are increased, the flow of fluid increases (both water, oil, and gas). This is due to increased conductivity in the fracture which allows the fluid to flow more quickly. For the duration of this study, the fracture permeability and fracture aperture are combined into one variable – the natural fracture conductivity. As the number of natural fractures in the grid is increased, the volume of fluid produced also increases. This is a result of larger fracture networks within the grid. As natural fractures are added to a finite volume (the grid) they are able to

interconnect more, and also increase their surface area within the grid blocks. Since fluid flow is governed by fracture networks in tight and fractured reservoirs, this increase in fracture surface area increases the flow of fluid (rates) and volume of fluid produced (cumulative plots). The fluid is able to flow at higher rates through the larger number of fractures and their connective networks.

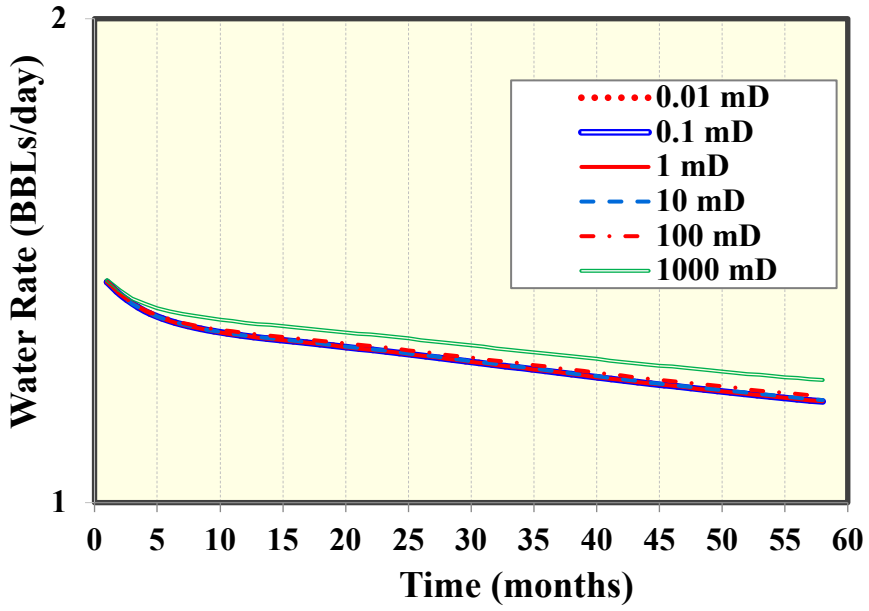

Figure 8: Water rate for the tight reservoir conceptual model with varying natural fracture permeability (0.01 mD to 1000 mD). Floor cutoff natural fracture permeability determined to be 10 mD for this model. The plot is shown on a log plot for water rate (BBLs/day).

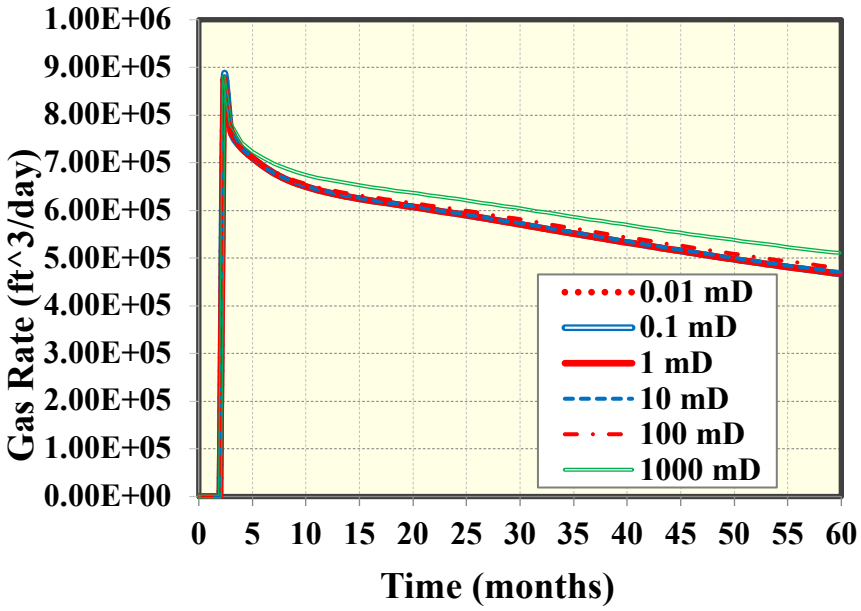

Figure 9: Gas rate for the tight reservoir conceptual model with varying natural fracture permeability.

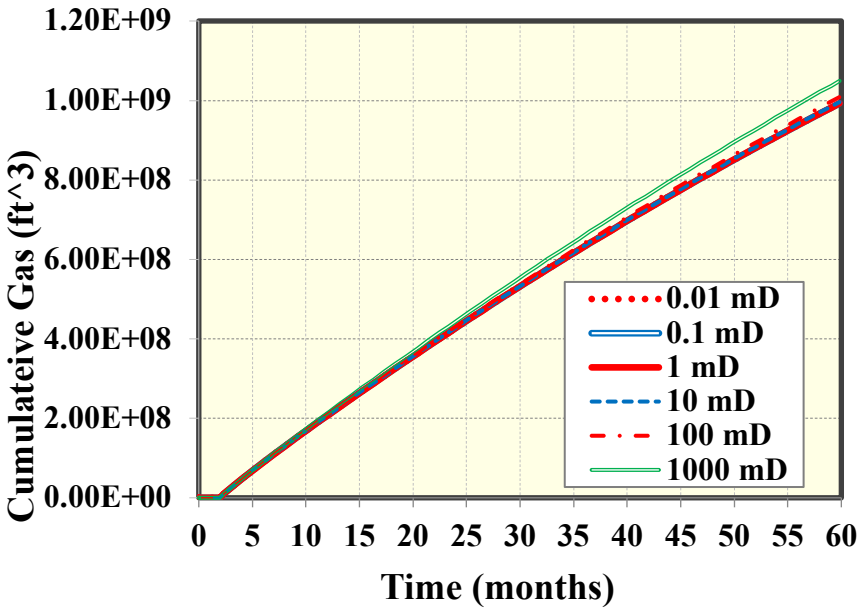

Figure 10: Cumulative gas production for the tight reservoir conceptual model while varying natural fracture permeability.

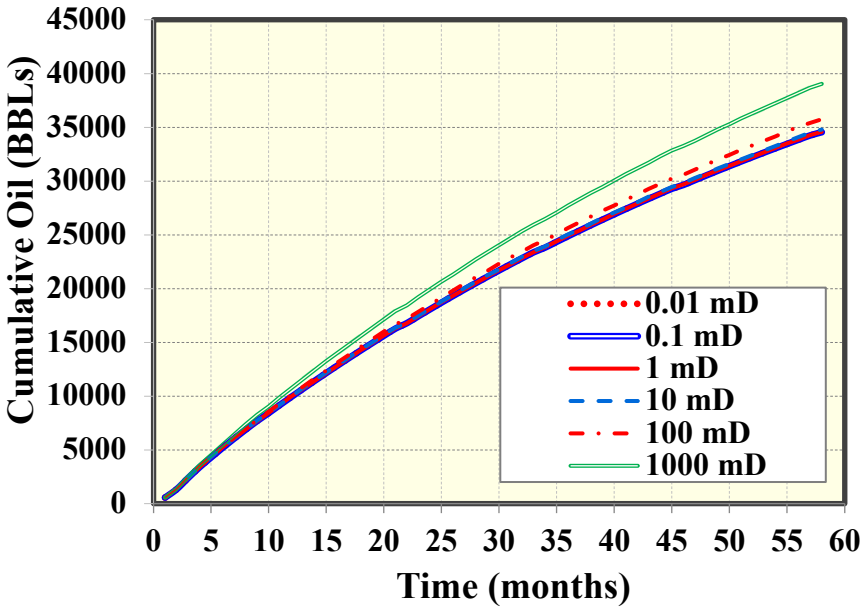

Figure 11: Cumulative oil production for the tight reservoir conceptual model with varying natural fracture permeability (0.01 mD to 1000 mD).

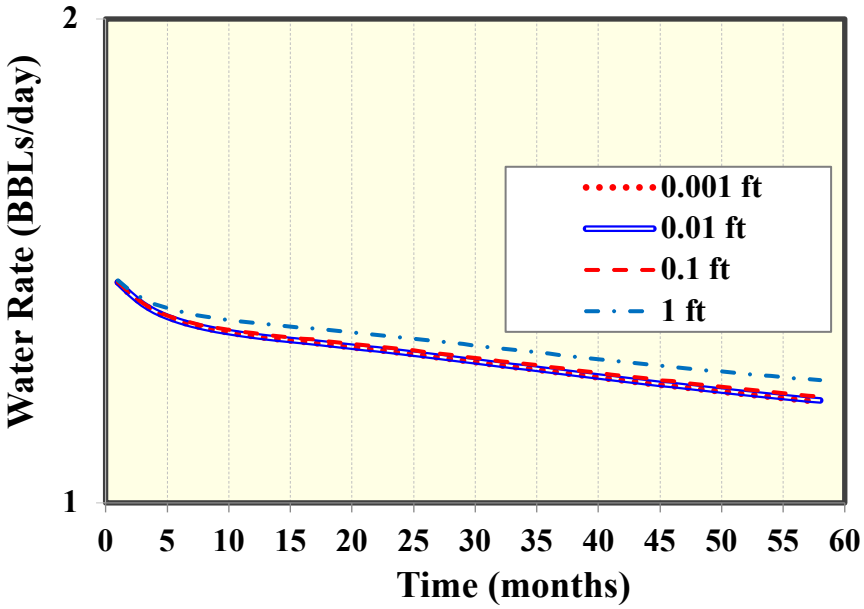

Figure 12: Water rate for the tight reservoir conceptual model with varying natural fracture aperture (0.001 ft to 1 ft). Floor cutoff aperture determined to be 0.01 ft for this model. The plot is shown on a log plot for water rate.

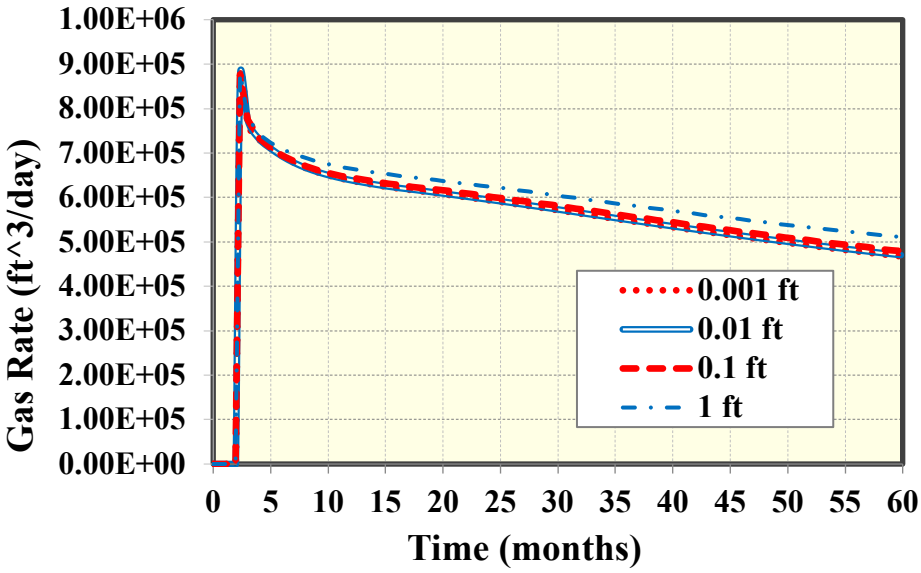

Figure 13: Gas rate for the tight reservoir conceptual model with varying natural fracture aperture.

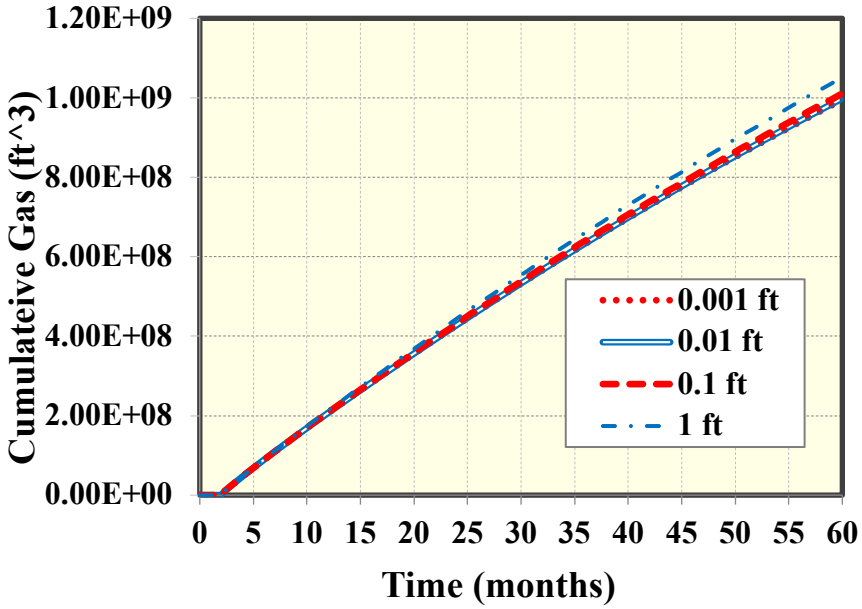

Figure 14: Cumulative gas production for the tight reservoir conceptual model while varying natural fracture aperture.

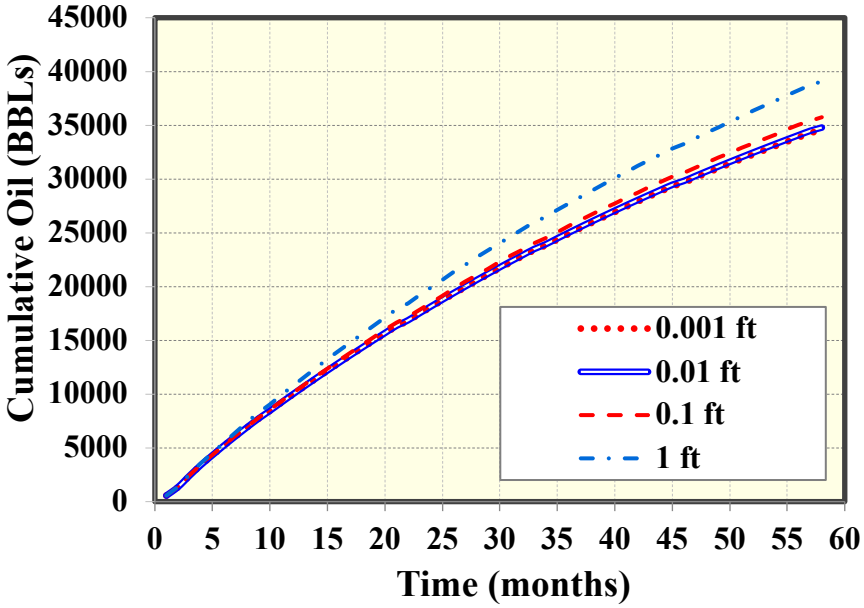

Figure 15: Cumulative oil production for the tight reservoir conceptual model with varying natural fracture aperture (0.001 ft to 1 ft). Floor cutoff aperture determined to be 0.01 ft for this model.

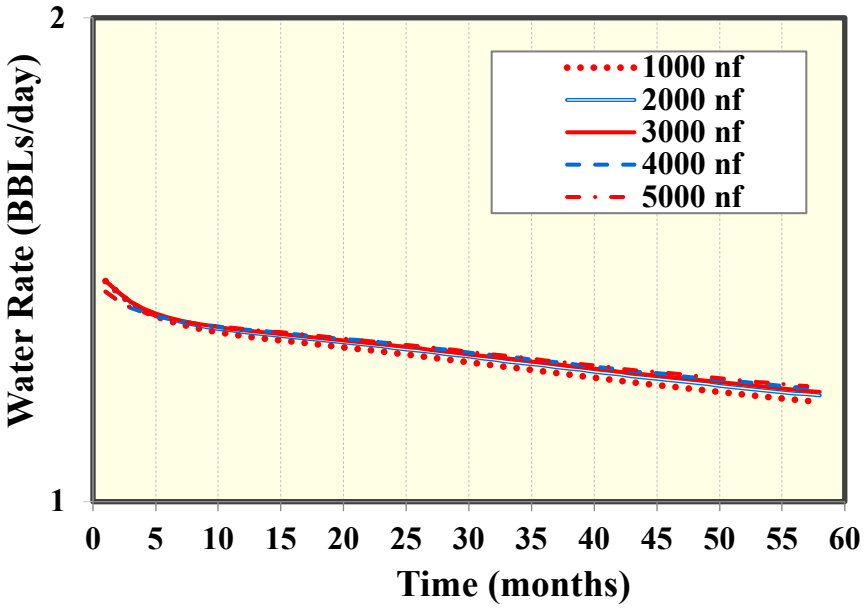

Figure 16: Water rate for the tight reservoir conceptual model with varying natural fracture number (1000 fractures to 5000 fractures). The plot is shown on a log plot for water rate (BBLs/day).

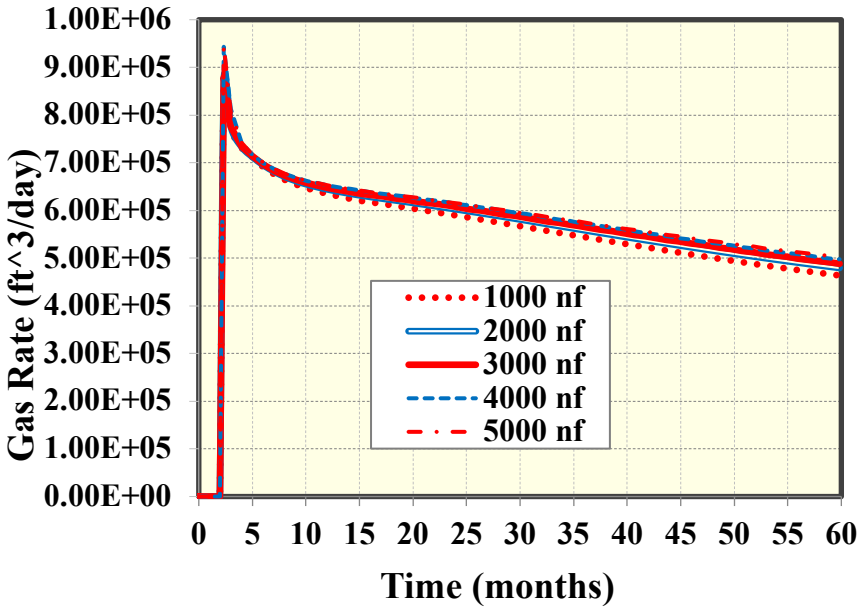

Figure 17: Gas rate for tight reservoir conceptual model varying natural fracture number

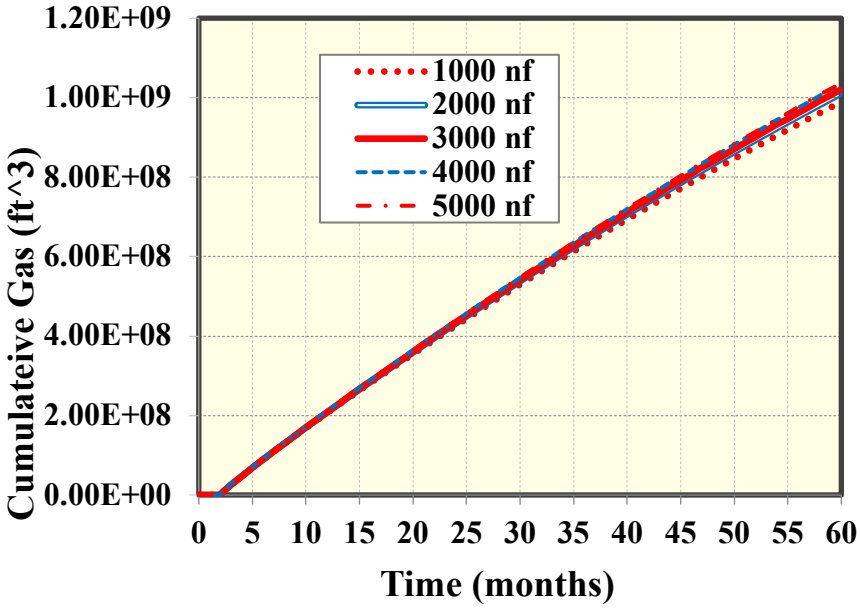

Figure 18: Cumulative gas production for the tight reservoir conceptual model while varying the number of natural fractures on the grid.

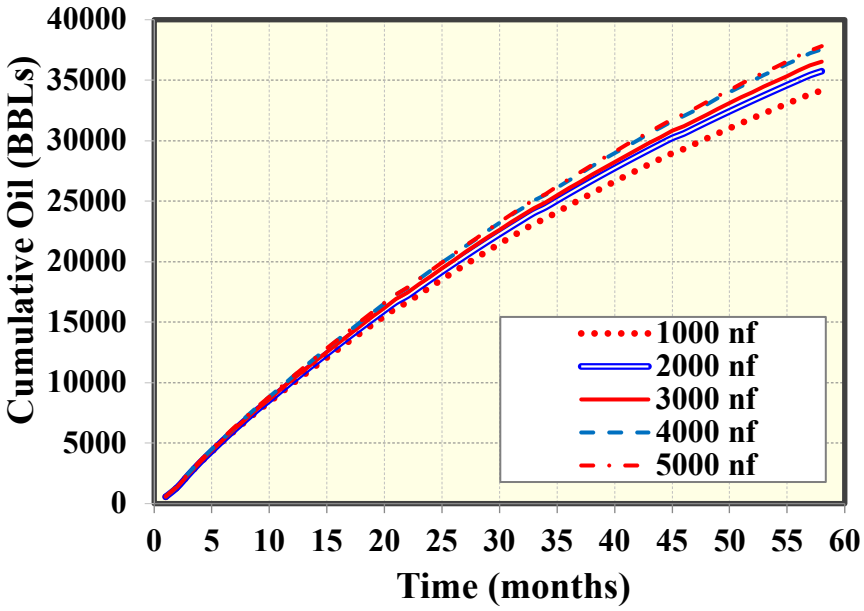

Figure 19: Cumulative oil production for the tight reservoir conceptual model with varying natural fracture number (1000 fractures to 5000 fractures).

There were cutoff values (ceilings and floors) where a dependent variable (water rate, gas rate, cumulative gas, or cumulative oil) no longer varied as that parameter was further increased or decreased. Ceiling cutoffs were defined where increasing the parameter no longer affected output variables. Floor cutoff were defined where decreasing the parameter no longer affected output variables.

Figure 20 and *Figure 21* show the pressure distributions in the reservoir at time t=3.5 months (first time step), and time t=58 months (final time step). It is evident the majority of the pressure loss in the system is in the nearby well region, resulting from the hydraulic fractures.

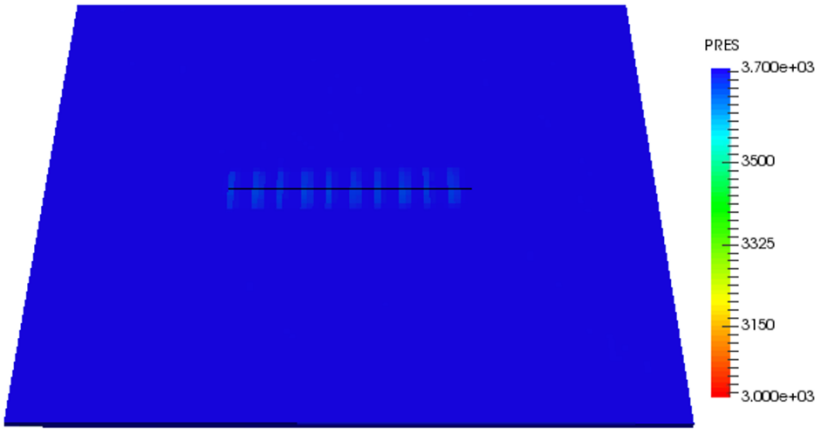

Figure 20: Pressure distribution at initial time, t=0.

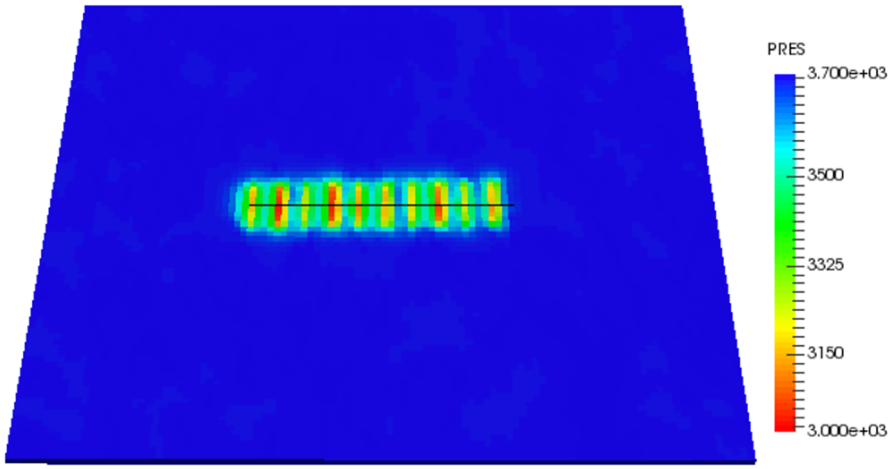

Figure 21: Pressure distribution at final time step, t=58 months of production.

2.1-5 Sensitivity Analysis

Figures 22-25 are the plots of the sensitivities of water rate, gas rate, cumulative gas, and cumulative oil production with varying number of natural fractures, natural fracture permeability, and natural fracture aperture. Density was the most sensitive variable

with respect to water rate, gas rate and cumulative gas. The cumulative oil sensitivity plot was relatively equal, with all variables having similar variance.

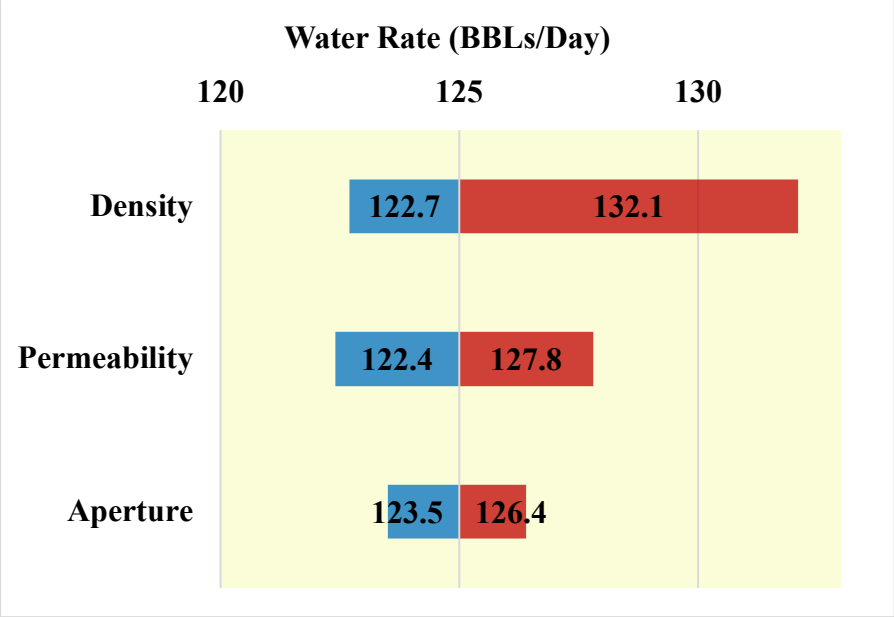

Figure 22: Water Rate sensitivity for the tight reservoir (low permeability) varying natural fracture density, permeability and aperture.

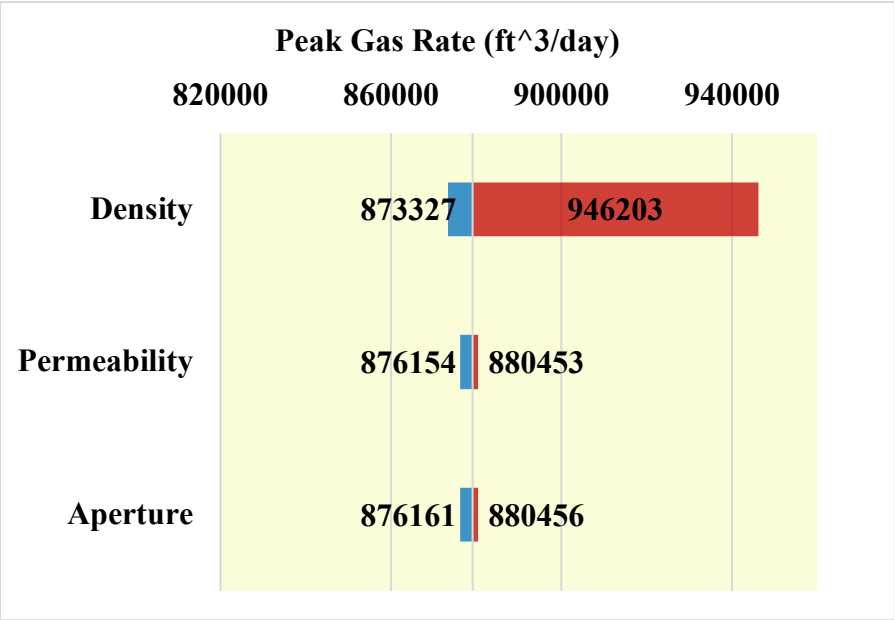

Figure 23: Gas rate sensitivity for the tight reservoir varying natural fracture density, permeability and aperture.

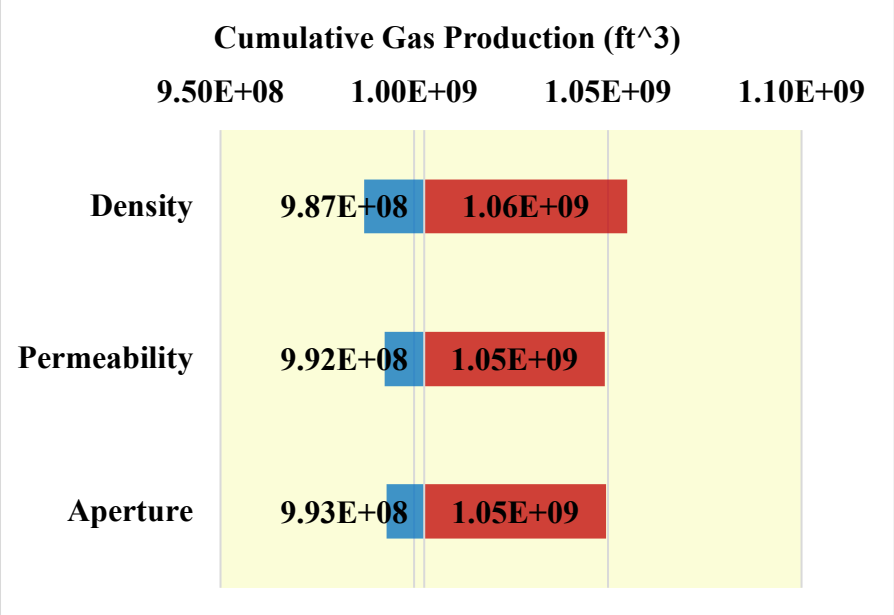

Figure 24: Cumulative gas sensitivity for tight reservoir varying natural fracture density, permeability and aperture.

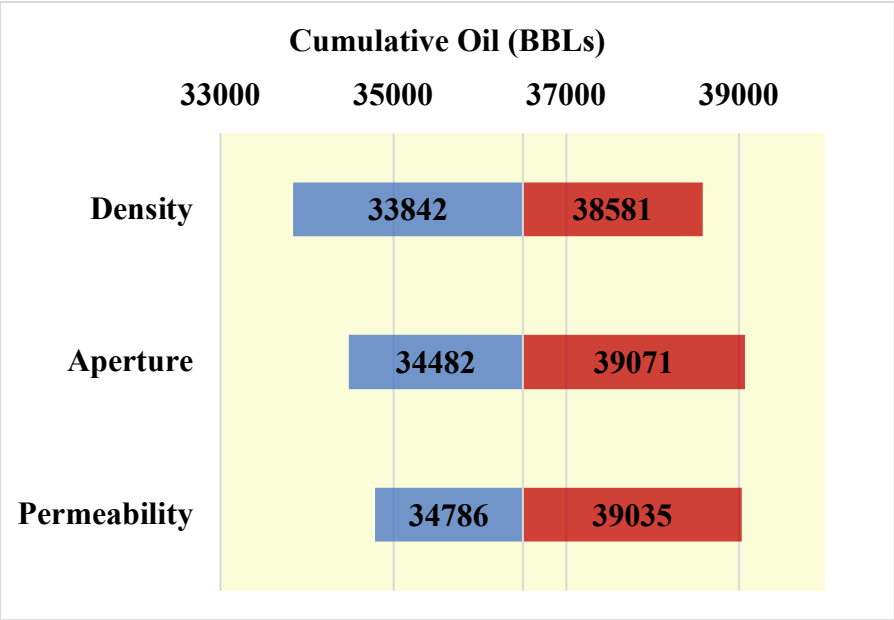

Figure 25: Cumulative oil sensitivity for the tight reservoir (low permeability) varying natural fracture density, permeability and aperture.

2.2 Carbonate Reservoir Model

2.2-1 Grid Model

A compositional model was used again for the carbonate reservoir sensitivity analysis. The composition of the fluid was the same as the fluid in the tight reservoir. The major difference between this model and the tight model was the matrix permeability, and the wellbore used was a vertical well as opposed to a horizontal well in the tight model. Table 6 summarizes the grid properties for this model.

Parameter	Value
Porosity, %	7.6-17.3
Permeability, mD	Matrix: 0.39-78
Kv/Kh	0.1
Initial Water Saturation	0.3
Reservoir Pressure, psi	3696
Avg. Reservoir Thickness, ft (z)	120
Fracture Height, ft	80-120
Natural Fracture Conductivity, md-ft	0.01-100

Table 6: Matrix and grid properties for the carbonate reservoir base model used in the sensitivity analysis

Figure 26 shows a visualization of the used grid. The grid is 100x90x6 in the (x, y, z) direction, respectively. The size of each grid block is 50 ft in the x and y-directions and 20 in the z-direction. The single vertical well can be seen in the center of the grid marked in red. This well penetrated through the first 4 layers (z-direction) of the model and the last 20 feet (1 layer of the grid) was completed by perforations.

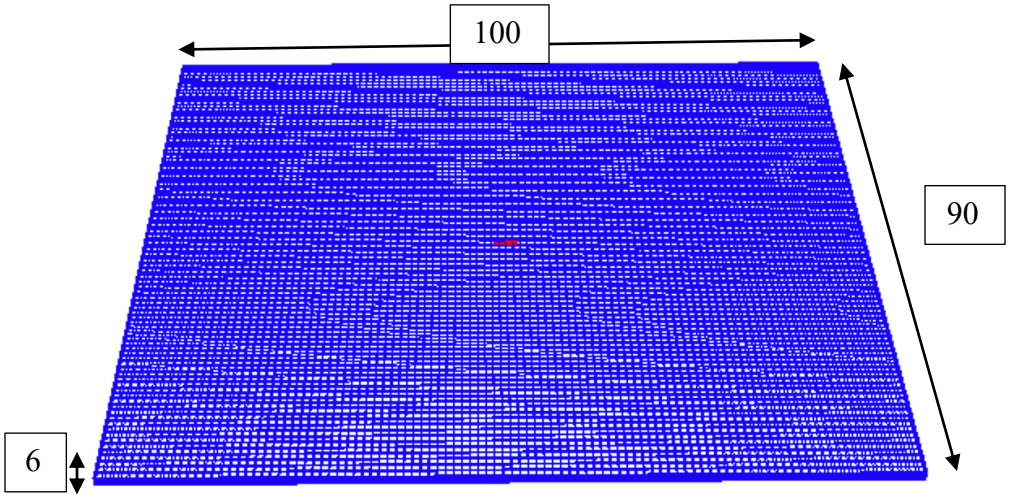

Figure 26: Visualization of the grid and wellbore for the carbonate conceptual model.

2.2-2 Results

The range of the variation of fracture properties can be found in Table 7. From the tight model, the natural fracture permeability and natural fracture aperture were combined into a fracture conductivity parameter which is measured in md-ft.

	Min	**Max**
Fracture Conductivity	0.01 md-ft	100 md-ft
Fracture Density	500	3000
Fracture Length	50 ft	800 ft
Aquifer Type	Fetkovich	Carter-Tracy

Table 7: Natural fracture properties and their ranges for the sensitivity study. Each of these were studied individual at a base case of 1 md-ft, 2000 natural fractures, and 200 ft. Aquifer types are also included with the base being Fetkovich and the sensitivity being Carter-Tracy

These properties were varied uniquely. Below in Figure 27-31, sensitivity to fracture conductivity can be seen on 5 dependent deliverables: water rate, gas rate, cumulative gas, water cut, and water-gas ratio. These models were run are using the Fetkovich aquifer model positioned beneath the matrix grid.

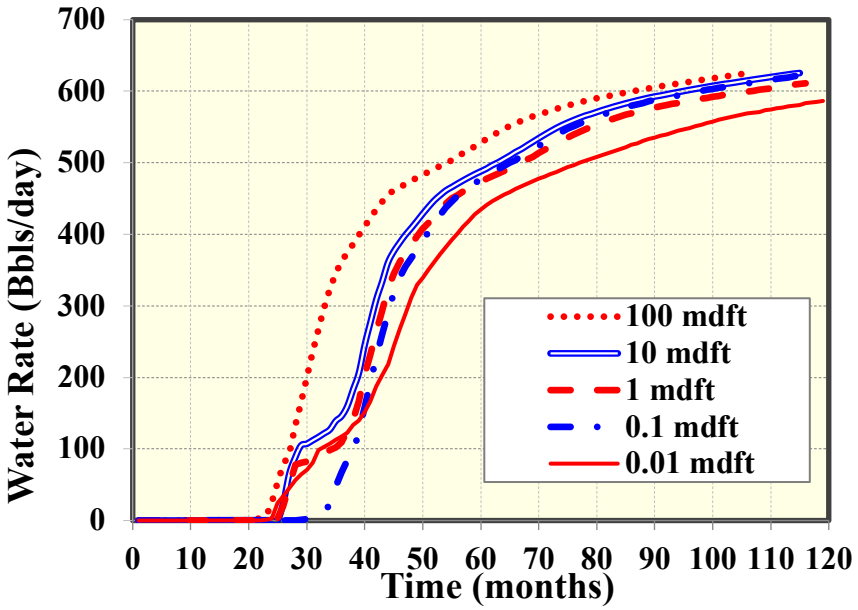

Figure 27: Water rate as a function of time while varying fracture conductivity.

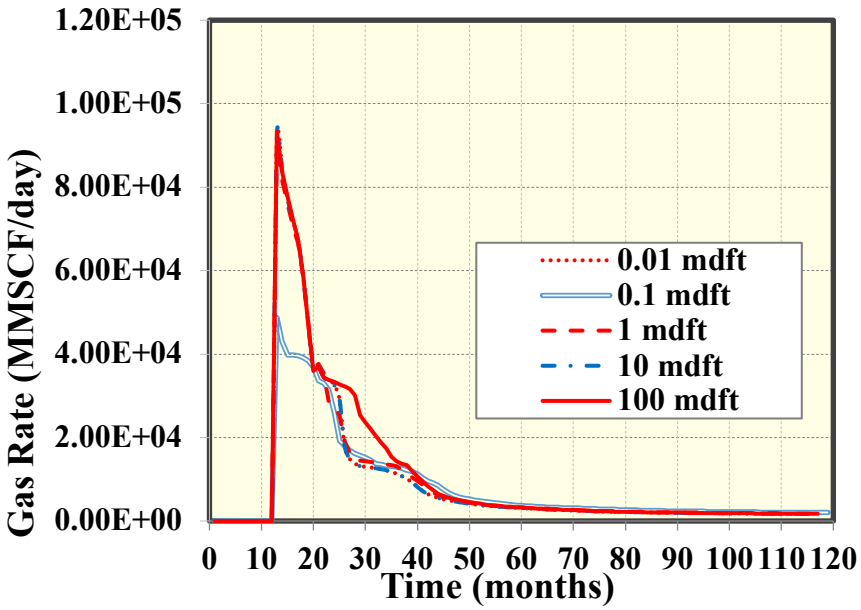

Figure 28: Gas rate as a function of time with varying natural fracture conductivities.

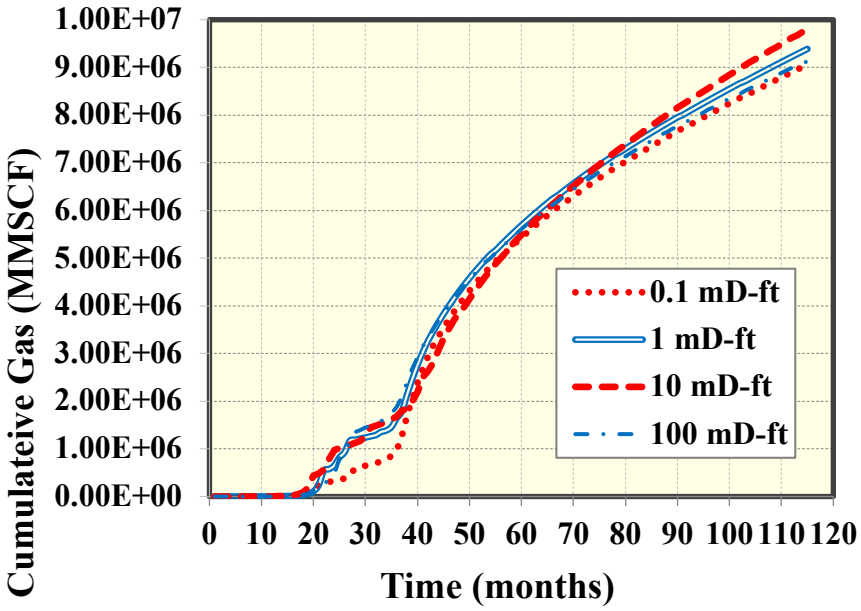

Figure 29: Cumulative gas production at varying conductivities for the carbonate model.

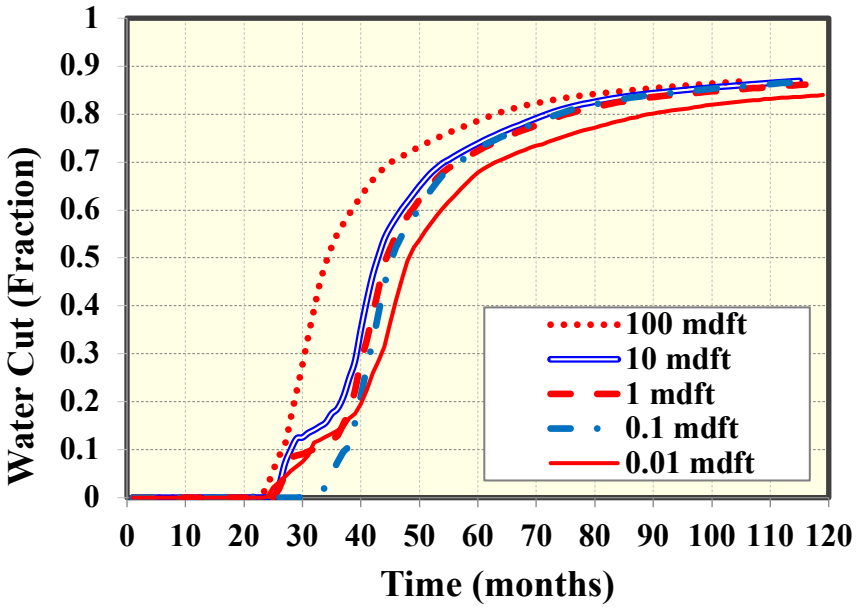

Figure 30: Water Cut as a function of production time while varying natural fracture conductivity.

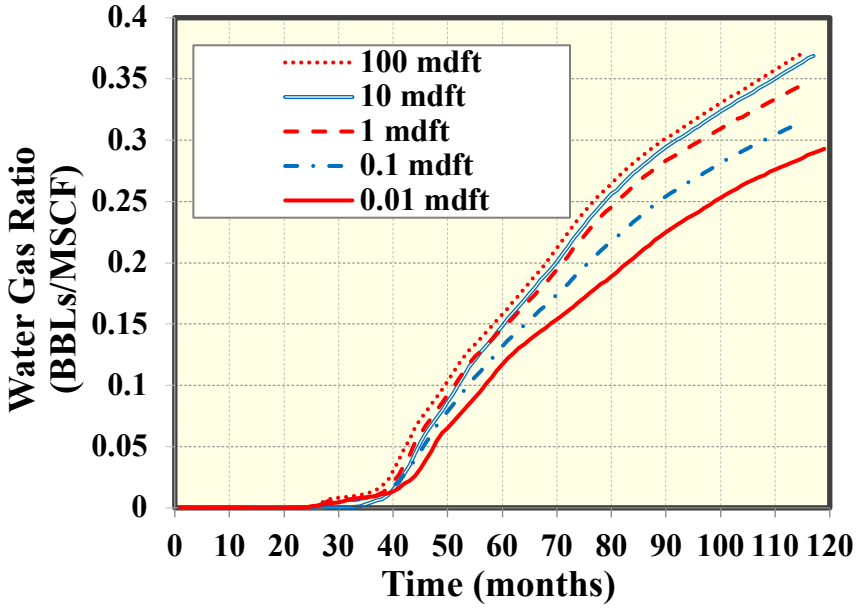

Figure 31: Water gas ratio as a function of production time while varying natural fracture conductivity.

From these plots, it is evident that water rate, water cut and water-gas ratio increases as fracture conductivity increases. The peak gas rate increases for the cases 1, 10 and 100 mD-ft. The declines of these curves are increase as the conductivity decreases: the decline for 100 mD-ft is less that 10 mD-ft, which is less than 1 mD-ft. Looking at the cumulative gas production, there is an interesting trend occurring. At the higher conductivity values (10 and 100 mD-ft), the early cumulative gas values are higher. However, overtime the 100 mD-ft case begins to decrease. This is due to the water intrusion into these highly conductive fractures. At early time, the gas rates peak quickly and are higher than the lower conductivities. However, as water intrudes it begins to saturate the natural fracture networks and leave the gas stranded. There is evidence of a cut-off conductivity for water-gas ratio. This is where increasing the fracture conductivity no longer affects the gas rate or water-gas ratio. These conductivities were at 10 md-ft. This convergence to a ceiling value for water-gas ratio can be explained by the fractures reaching nearly infinite

conductivity. At this infinite conductivity, increasing conductivity no longer proportionally increases the water-gas ratio. Sensitivities on the number of fractures in the grid were performed next. Their results can be found in *Figures 32-36*.

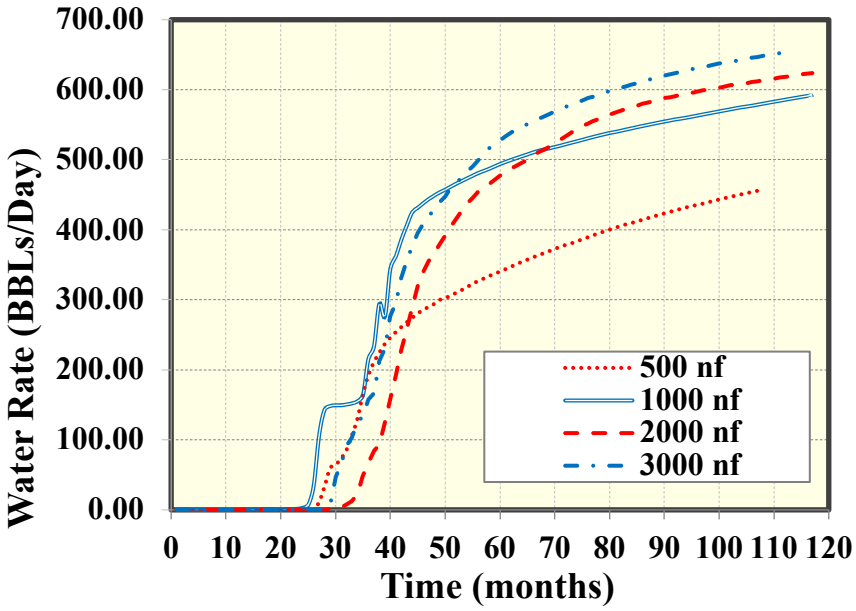

Figure 32: Water rate as a function of production history while changing natural fracture number.

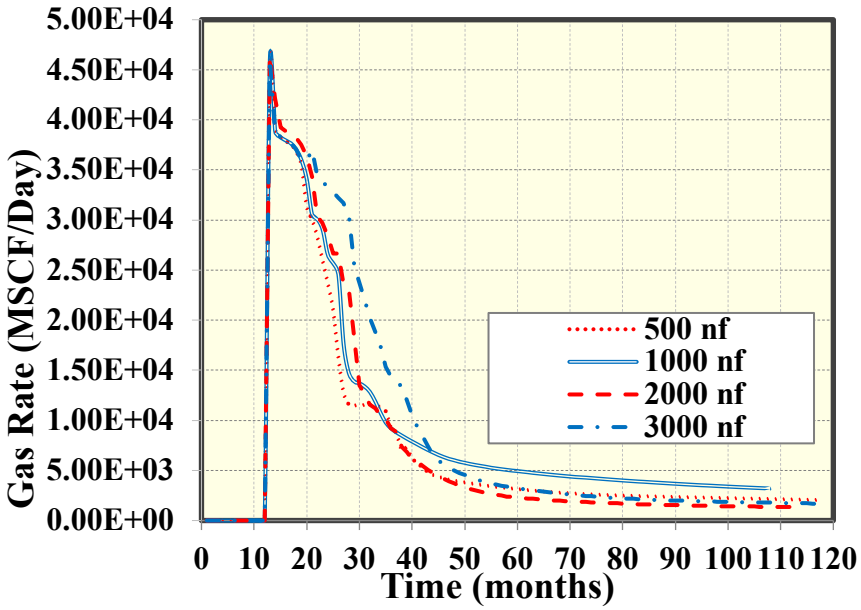

Figure 33: Gas rate as a function of production history with varying number of natural fractures.

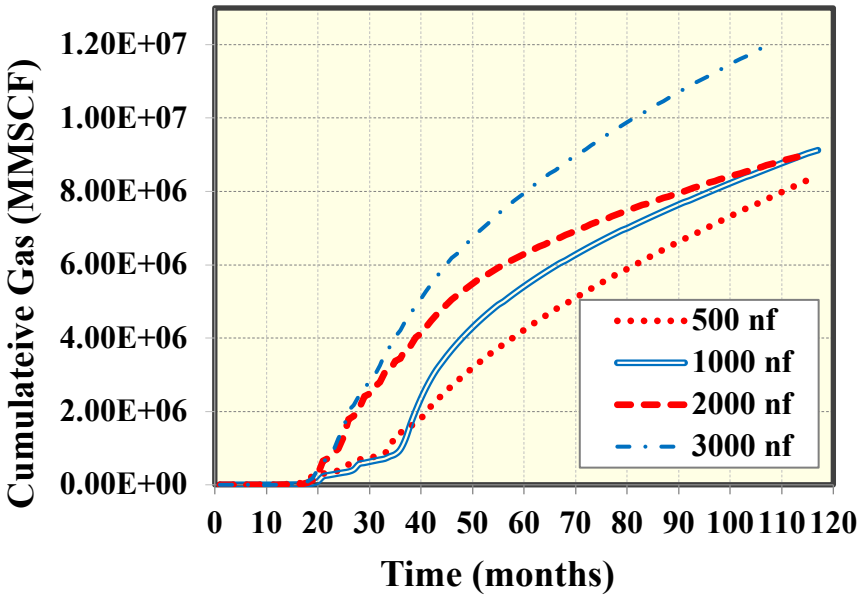

Figure 34: Cumulative gas production at varying number of natural fractures for the carbonate case.

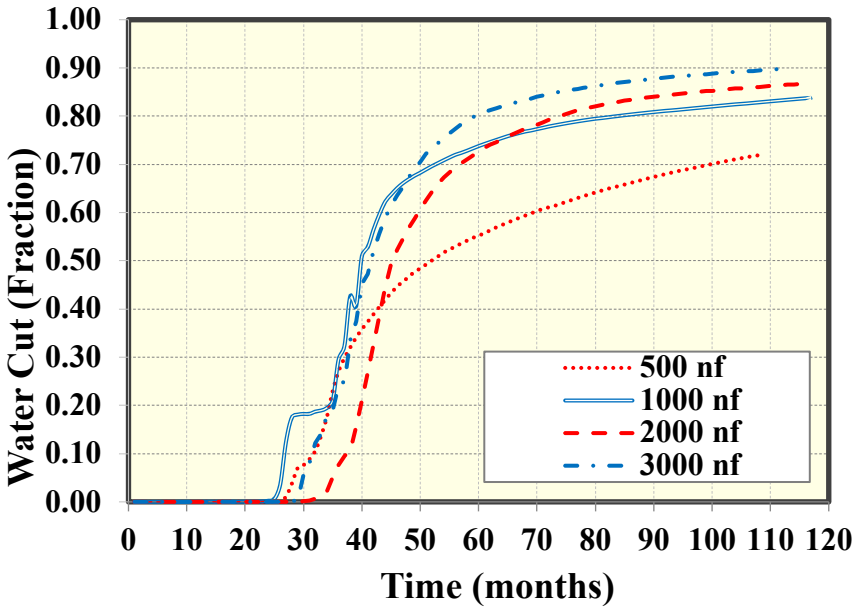

Figure 35: Water cut as a function of production time while varying number of natural fractures.

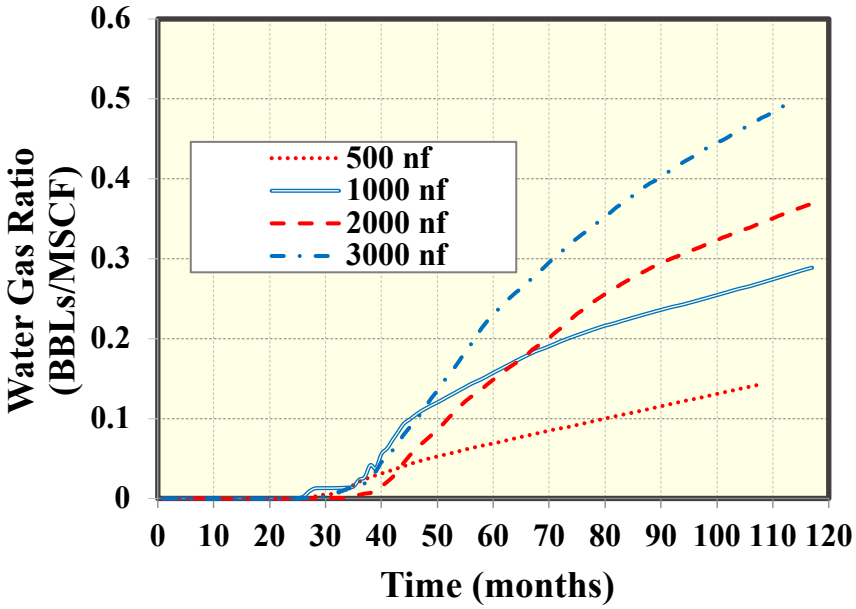

Figure 36: Water gas ratio as a function of number of natural fractures on the grid.

Once again, there is a clear relationship between increasing the number of fractures and its effect on water rate, water cut, and water-gas ratio. As we increase the number of fractures in the grid the water rate, water cut, and water-gas ratio increase. This increase in water rate, water cut, and water gas ratio can be explained by the increased natural fracture surface area in the grid and increased interconnectivity of the fractures. Adding more fractures, to a fixed volume, creates more highly conductive pathways for the fluid to flow through. Additionally, as more fractures are added, even at random, they have a higher probability of interacting with each other and creating a faster flow path to the wellbore. Due to the strength of the aquifer, as pressure decreases in the reservoir water invades these fractures and saturates them, further influencing more water flow to the wellbore. This explains the increase in the water producing rates, and ratios over time with an increasing number of natural fractures.

Gas rate, once again, appears to remain relatively constant with increasing natural fracture number. However, analyzing the cumulative gas curve, a similar trend to the conductivity case emerges. As the number of fractures on the grid increases, the initial cumulative productions for the 3000 natural fracture and 2000 natural fracture cases are higher than the 500 and 1000 natural fractures. However, over time the 2000 natural fracture case begins to decline. This is due to the water intrusion and gives another insight. As the surface area of these fracture and interconnectivity of these fractures increases, it increases our initial rate of production of hydrocarbons. However, it also increases the probability that these fractures will be close to the aquifer and give a faster flow path to the wellbore. In this case, the 3000 natural fracture case did not have a fast water breakthrough time. However, the 2000 natural fracture case did have a fast breakthrough time and the gas production quickly declined. This is evident through the decline in slope on the cumulative gas curve for the 2000 natural fracture case.

Finally, a sensitivity study was run for the length of these natural fractures. The natural fracture conductivity and number of natural fractures were held constant for this analysis. The results of the study can be found in *Figures 37-41*. There is, once again, a trend of higher water rate, water cut, and water-gas ratio with increase natural fracture length. This is due to more intersection among fractures and quicker water breakthrough due to increased volumetric flow of water across the reservoir through the natural fractures. Gas rate is held relatively constant at varying fracture lengths; however, analyzing the cumulative gas production plot shows similar trends to the conductivity, and number of fracture cases above. In the gas rate plot, there appear to be two outliers at 400 and 800 ft natural fracture lengths. However, this is just due to the proportional jump (from 100 to 200, 200 to 400, then 400 to 800) in the length of the fractures. These early peaks in gas rate correlates to the peak in *Figure 38*. The 400 and 800 ft fracture cases reflect the proportional jump in surface area within the fracture network. The cumulative gas plots show an early jump in the longer length natural fractures (400 and 800 ft). However, at 52 months the 400 ft case crosses over the 800 ft case on the cumulative gas plot. Once again, this shows evidence of the tradeoff between larger natural fracture surface area and interconnectivity within the fracture networks. As the surface area and interconnectivity increase, the gas production will increase as well; however, there is a risk of faster water intrusion if these natural fractures interact with the aquifer or are very close to the wellbore. The faster water breakthrough occurs for the 800 ft fracture case and the gas production declines.

Similar reasoning holds for this varying natural fracture length as for varying the number of natural fractures. As the length of the natural fractures are increased more an increased surface area of the fixed volume grid is filled with fracture networks. This increase creates more highly conductive pathways for the water to flow through.

Additionally, longer natural fractures increase the probability of intersection with other fractures on the grid allowing for more highly-transmissible pathways for the intruding water to flow to the wellbore. This is further confirmed by the steeper decline in the 400 and 800 ft natural fracture cases. Water is able to flood these fractures and breakthrough to the well quicker in these cases. This is the same reasoning for the natural fracture density above. These gas rates were overcome by an increase in water rate after the breakthrough of the aquifer. Further analysis into the breakthrough time for each case was conducted next.

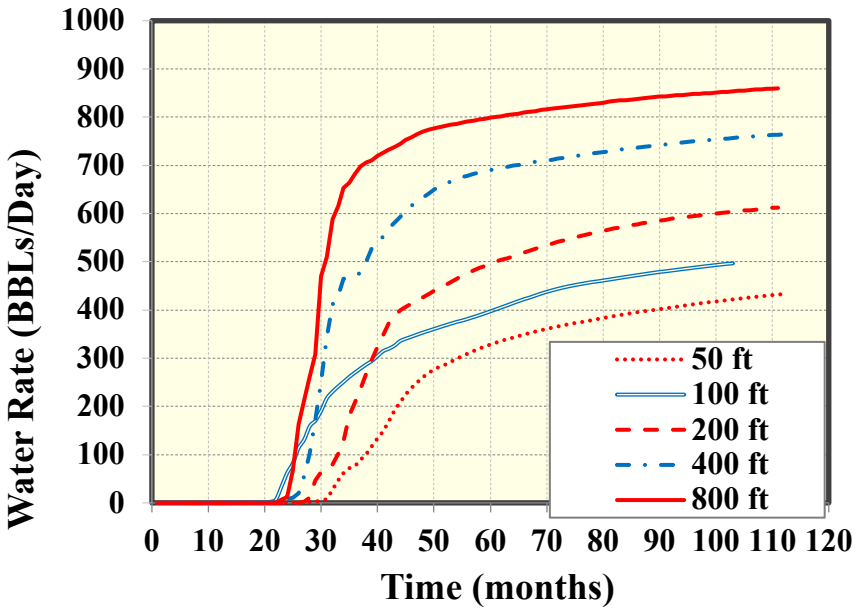

Figure 37: Water rate as a function of production time while varying the natural fracture length (ft).

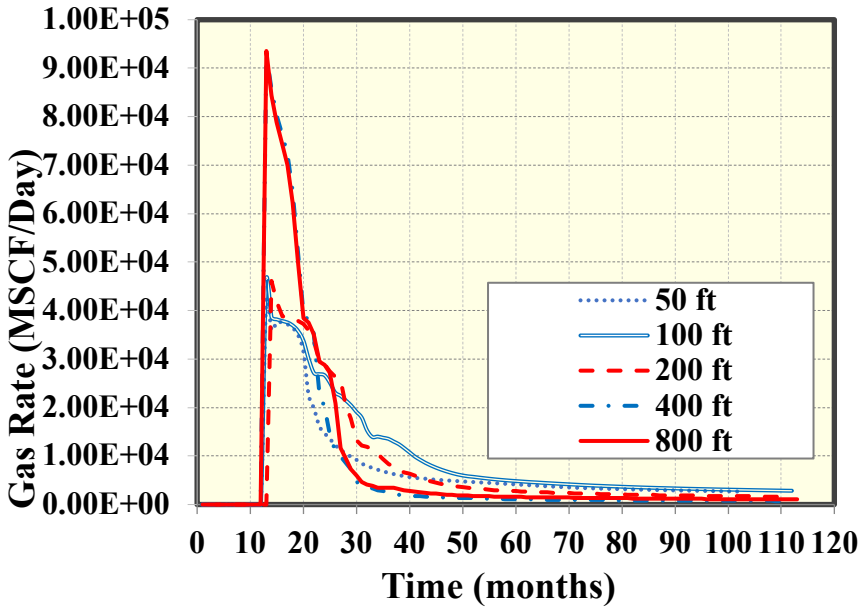

Figure 38: Gas rate as a function of production time while varying natural fracture length (ft).

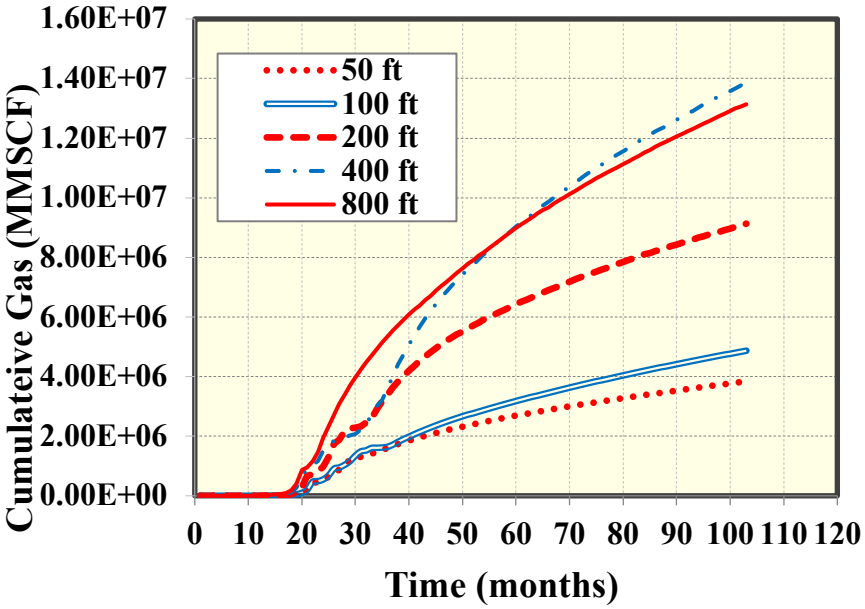

Figure 39: Cumulative gas production varying the natural fracture lengths for the carbonate case

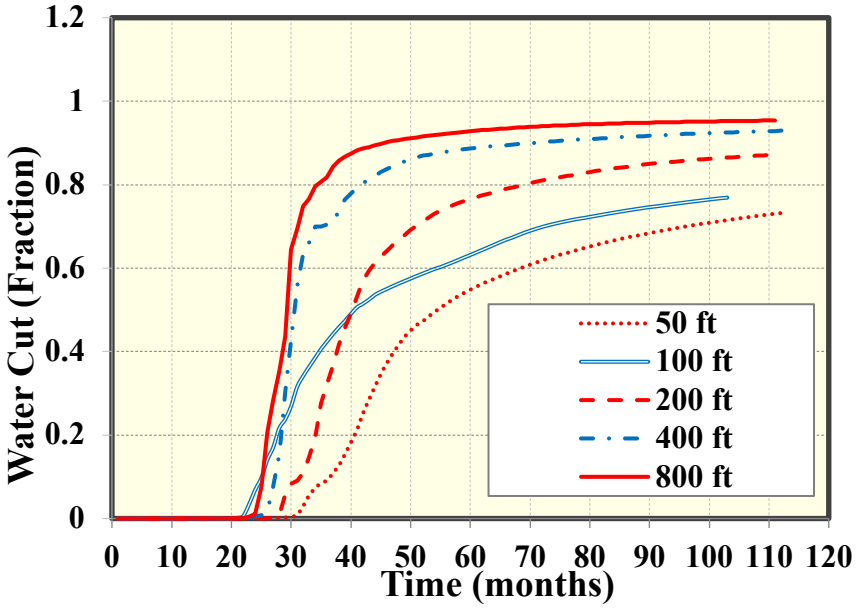

Figure 40: Water cut as a function of production time while varying natural fracture length (ft).

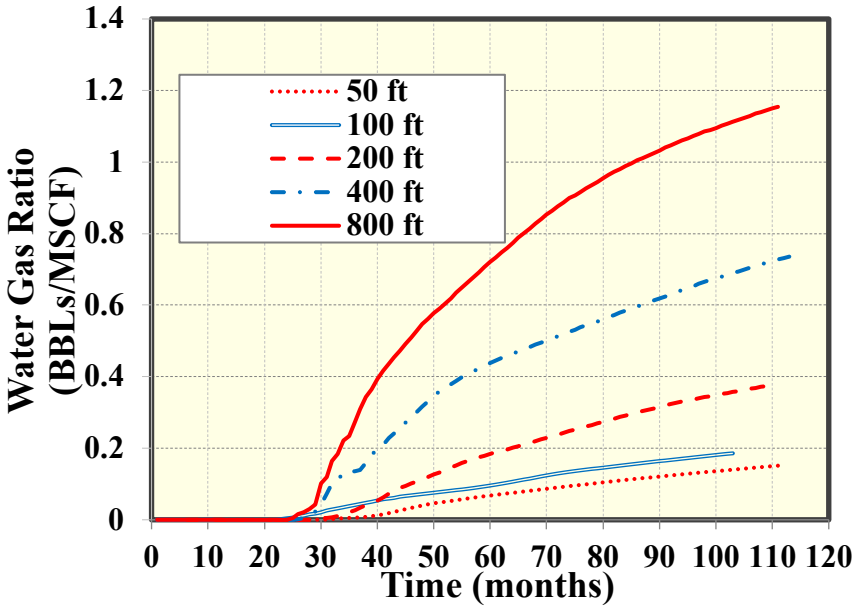

Figure 41: Water gas ratio as a function of production time while varying natural fracture length (ft)

Figure 42 and *Figure 43* show the pressure distributions in the reservoir at time t=3.5 months (first time step), and time t=120 months (final time step). At the final time step, there is clear evidence of water intrusion as the drainage radius is no longer radial. This is due to the invasion of the aquifer into the reservoir.

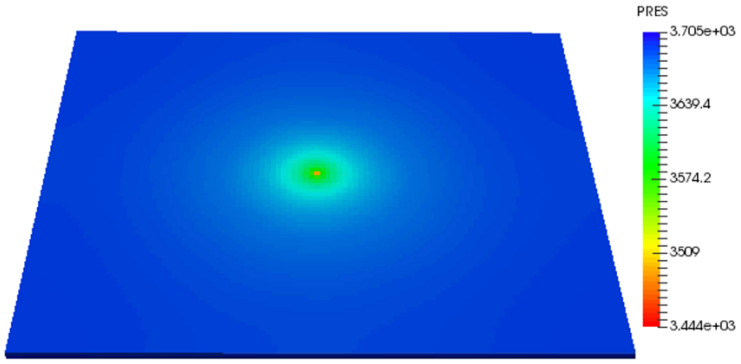

Figure 42: Pressure distribution at t=3.5 months in the reservoir.

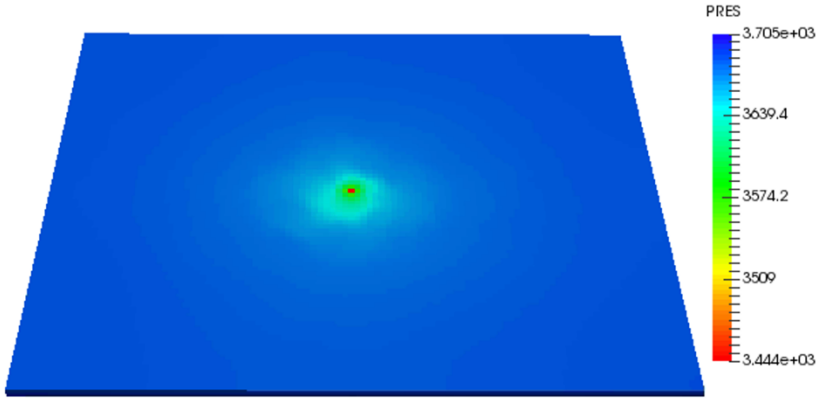

Figure 43: Pressure distribution at the final time step t=120 months of production

2.2-3 Aquifer Breakthrough Time

The aquifer breakthrough time was discerned by the change in curvature of the water rate and water cut plots from the above sensitivities. *Figure 44* highlights the estimated breakthrough time from a scenario with natural fracture conductivity equal to 1 md-ft, natural fracture length equal to 200 ft and 2000 natural fractures in the reservoir.

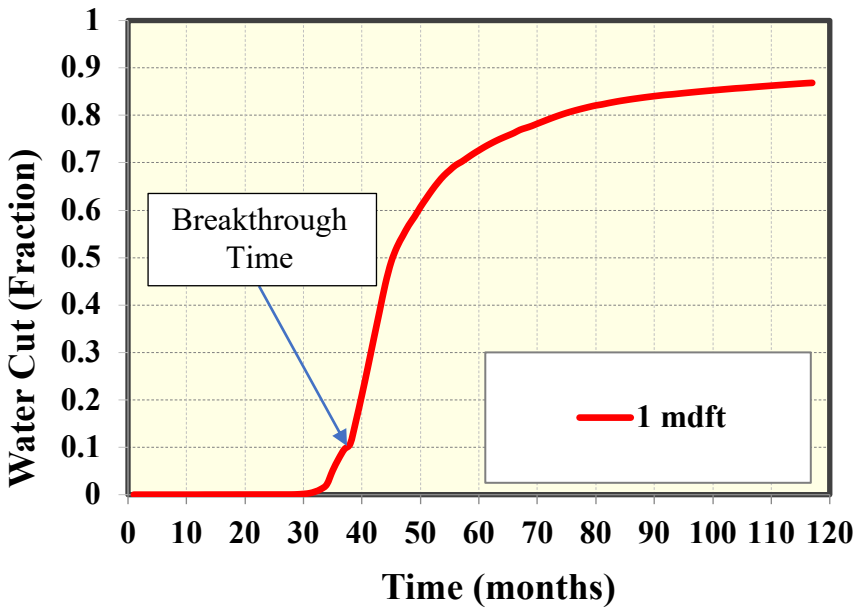

Figure 44: Example illustrating the estimation of aquifer breakthrough into the wellbore for a fracture sensitivity containing natural fracture conductivity equal to 1 md-ft, 200 ft natural fracture length, and 2000 natural fractures in the reservoir model.

Production began at time equal to 20 months. The point here indicates a breakthrough time of 18 months after production (t=38 months). This technique was confirmed using a visualization software which shows the water saturation in fractures surrounding the wellbore. *Figure 45* shows a snap shot at the initial time (t=0) and *Figure 46* shows the saturations at 18 months of production.

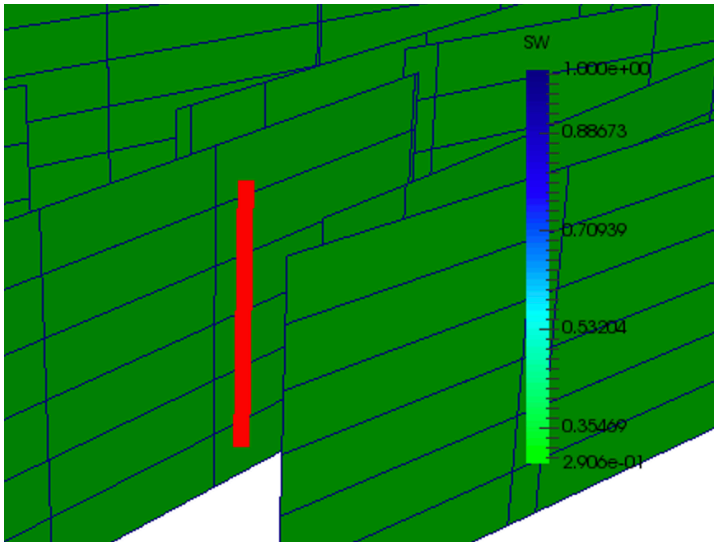

Figure 45: Initial water saturation in the natural fractures near the wellbore (at t=0).

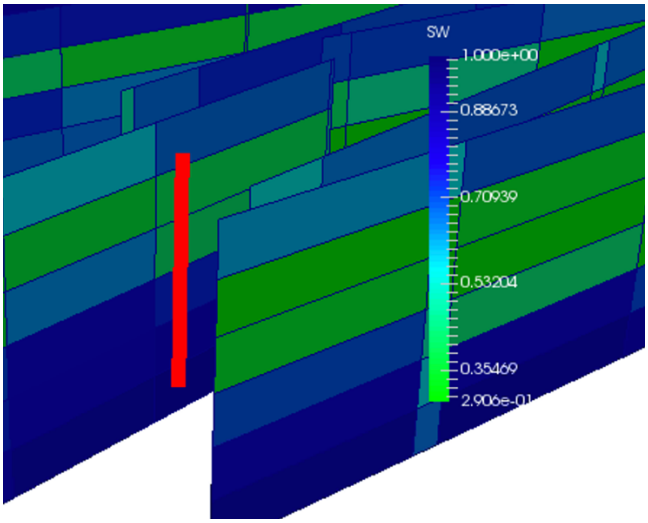

Figure 46: Visualization showing the natural fracture water saturations near the wellbore (at t=18 months0). Fractures near the bottom of the model indicate water saturations equal to, or exceeding, 0.95.

2.2-4 Sensitivity Analysis

Table 8 shows the ranges of the differing sensitivities presented below. The base case, used for comparison in the tornado diagrams in highlighted in bold.

Parameter	Minimum	Base	Maximum
Fracture Conductivity	0.01 md-ft	**1 md-ft**	100 md-ft
Fracture Length	50 ft	**200 ft**	800 ft
Fracture Density (Number)	500 Fractures	**2000 Fractures**	4000 Fractures

Table 8: Sensitivity ranges for the sensitivity study comparing natural fracture properties to water production metrics.

Tornado diagrams were developed for each of the above scenarios to help illustrate the impact of natural fracture properties on water production and breakthrough time. The tornado diagram for water breakthrough time is below in Figure 47.

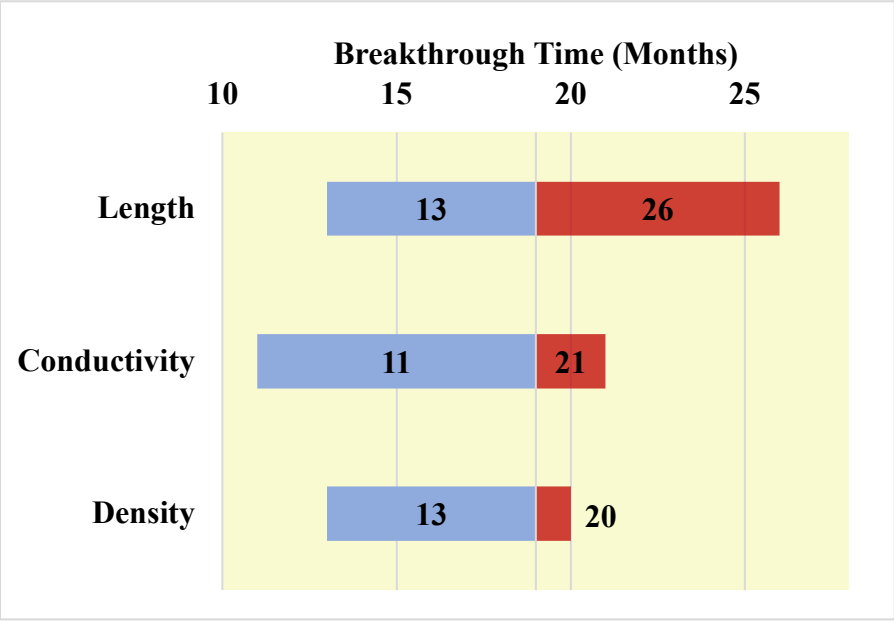

Figure 47: Tornado diagram representing the sensitivity of varying length, density and transmissibility on water breakthrough time. The base case for this study was 1 md-ft, 200 ft fracture length and 2000 natural fractures.

The highest sensitivity is to fracture length for the water breakthrough time. *Figure 48* shows the tornado diagram for the water rate sensitivity. *Figure 49* shows the tornado

diagram for the water cut sensitivity. *Figure 50* shows the tornado diagram for the peak gas rate sensitivity. *Figure 51* shows cumulative gas sensitivities. *Figure 52* shows the tornado diagram for the water-gas ratio sensitivity.

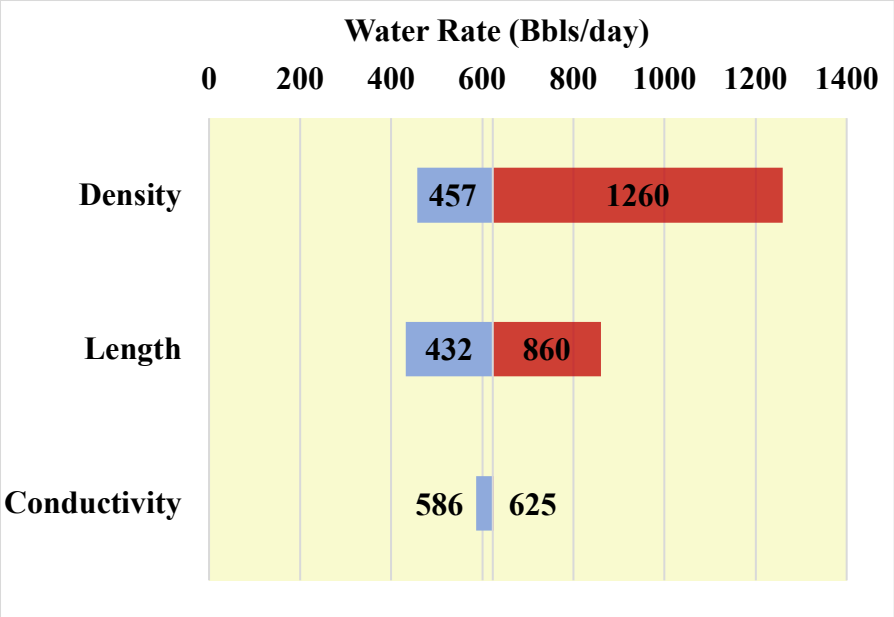

Figure 48: Water rate sensitivity study showing the ranges for differing fracture conductivities, natural fracture lengths and natural fracture density.

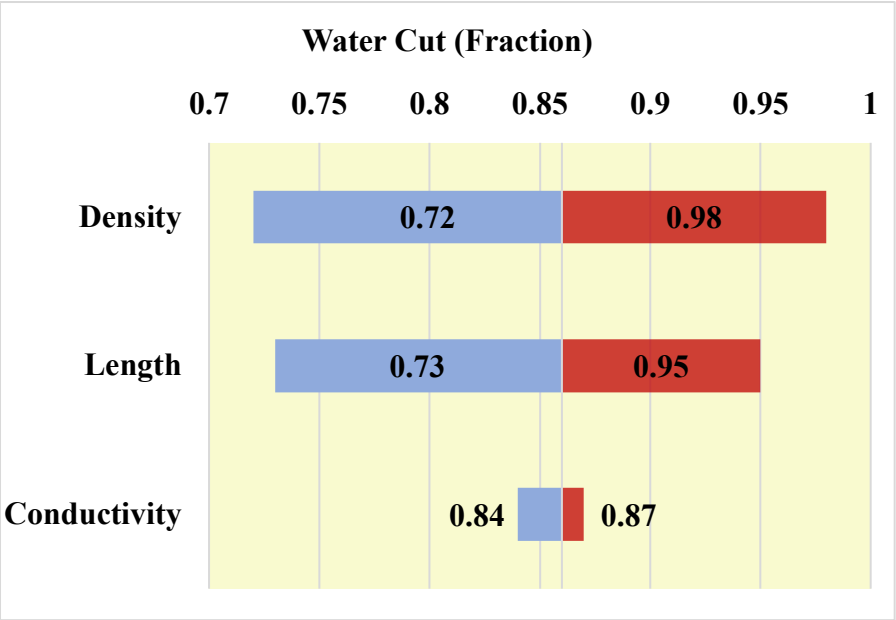

Figure 49: Water cut sensitivity study showing the ranges for differing fracture conductivities, natural fracture lengths and natural fracture density. The ranges for these parameters are found in Table 6 above.

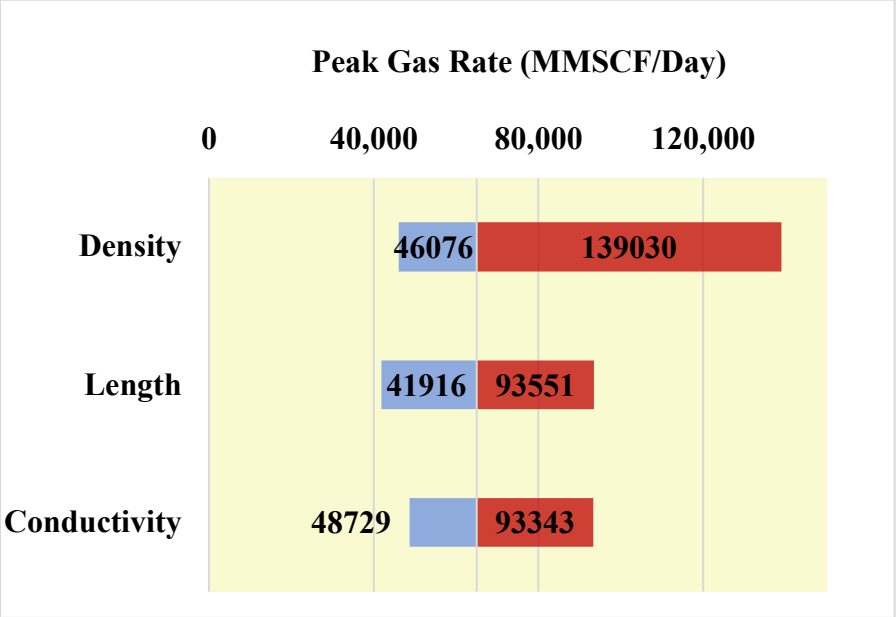

Figure 50: Peak gas rate sensitivity study showing the ranges for differing fracture conductivities, natural fracture lengths and natural fracture density. The ranges for these parameters are found in Table 6 above.

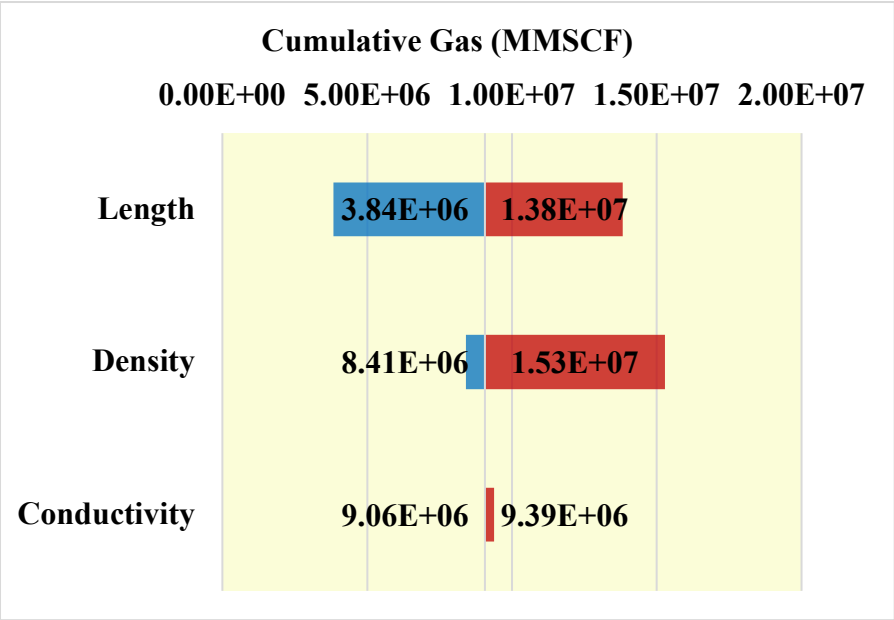

Figure 51: Tornado diagram representing sensitivity of natural fracture length, number and conductivity to Cumulative Gas Production.

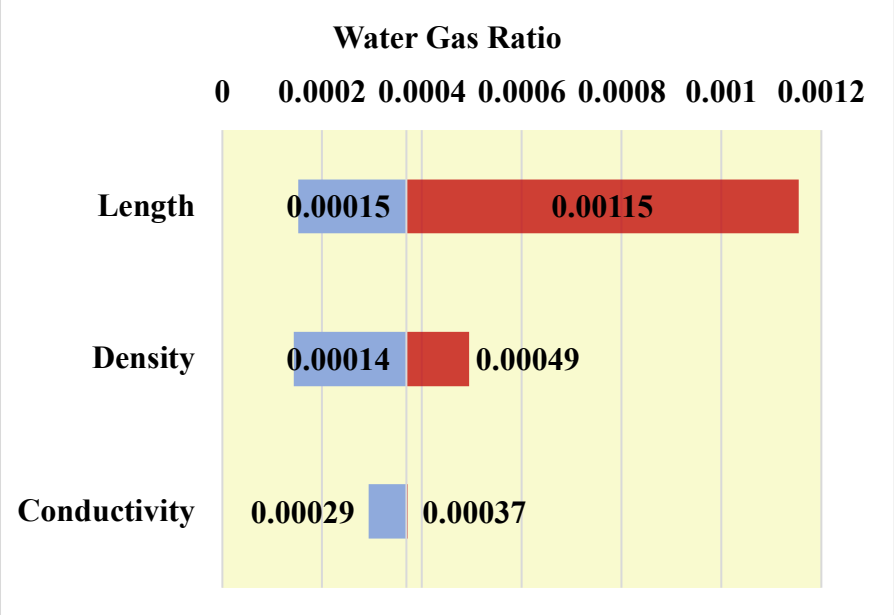

Figure 52: Water-gas ratio sensitivity study showing the ranges for differing fracture conductivities, natural fracture lengths and natural fracture density. The ranges for these parameters are found in Table 6 above.

The study showed that the highest sensitivity variable was fracture density followed by fracture length. This is defined as the number of fractures within the grid. Natural fracture length showed the second highest sensitivity. These two parameters, when maximized in the study, increased the number of fracture interactions and fracture contact surface of water across the grid. For longer fractures, they have a higher probability of crossing over each other, on a finite grid, than shorter fractures. Additionally, a higher number of fractures in the grid would increase the fracture interaction network and govern the flow rate of fluid throughout the grid. Conductivity showed the lowest sensitivity throughout this study. This is explained by the increase in isolated fractures in the higher conductivity case. Because there is not an increase in the number of fractures, or their length, there is a higher probability of isolation among the highly conductive fractures. Therefore, even though the fluid may flow more easily through higher conductivity fractures, they do not contribute to the network as a whole, or the well's production. This can significantly slow the flow of water to the wellbore if fractures are not long enough or dense enough to carry water close to or across the wellbore.

2.2-5 Aquifer Types

This section is dedicated to compare the different aquifer types. All natural fracture properties, matrix properties, and aquifer properties were held constant during this analysis. The properties for each aquifer type are in Table 9, below. The only variable was the type of aquifer model used. From Figure 53, it is clear there is a difference in the values that the model produced.

Aquifer Property	Fetkovich	Carter-Tracy
Height (ft)	120	120
Porosity (%)	10	10
Permeability (mD)	20	20
R/r ratio	100	100

Table 9: Aquifer properties used for the Fetkovich and Carter-Tracy comparison study.

The Fetkovich model had lower water rates for all values past 24 months of production. Their approaches are similar, as described in Chapter 1 above, however the Fetkovich simplification ignores the transient flow regime (Fetkovich 1971). Additionally, Fetkovich is for finite aquifer models while Carter-Tracy adopts an infinite aquifer which is stronger than a finite aquifer (Carter-Tracy 1960; Fetkovich 1971).

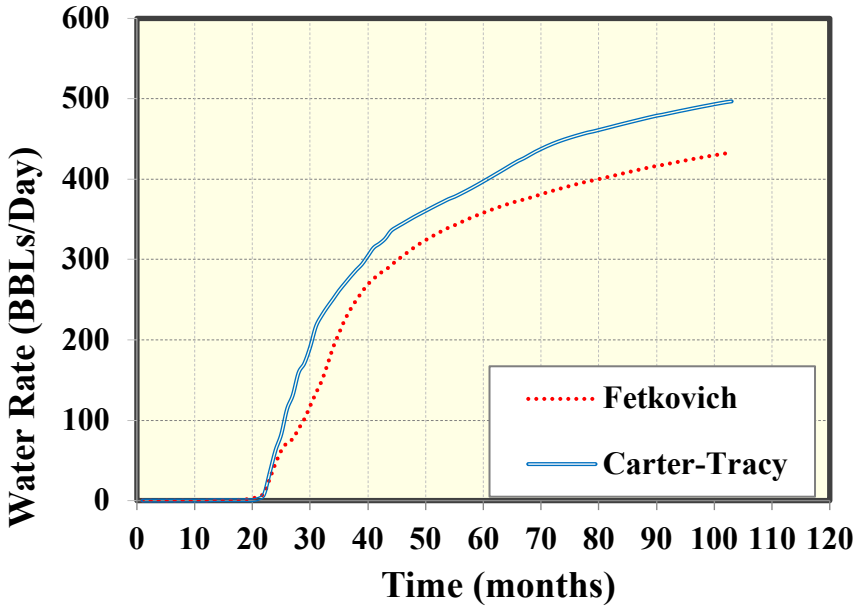

Figure 53: Fetkovich model compared to the Carter-Tracy aquifer model

Figures 54 and *55* are the water saturation distributions at t=0 and t=120 months of production. From these figures, there is clear evidence of water intrusion through the

natural fracture network. The uneven distribution of fractures consolidating towards the wellbore, illustrates how these networks, when interacting with an aquifer near the wellbore, can influence production by increasing water rates over time.

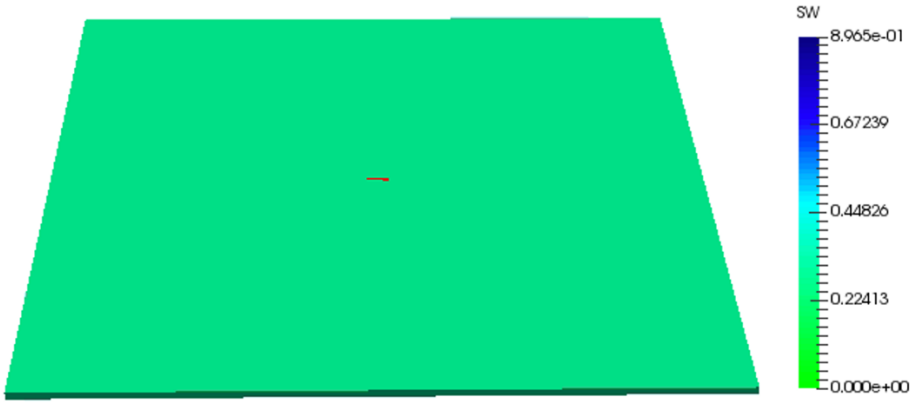

Figure 54: Water saturation for the carbonate model at the initial time step (t=0 months).

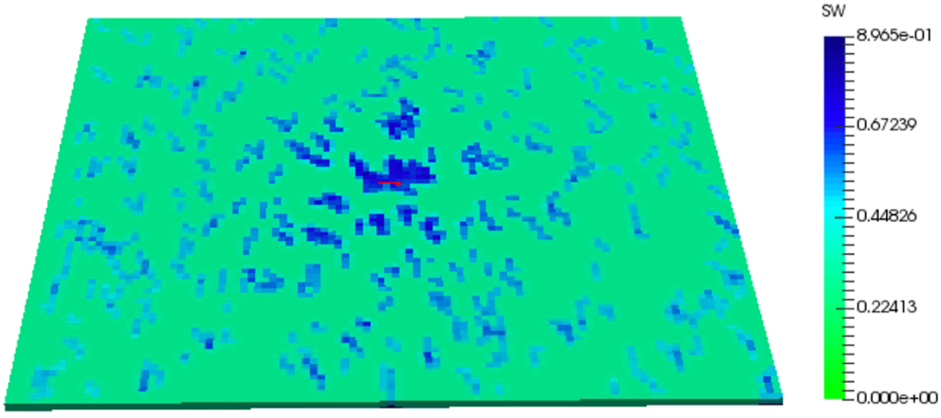

Figure 55: Water saturation for the carbonate model at the final time step (t=120 months).

Chapter 3: Field Study

3.1 Wells Information

The final portion of this project corresponded to a field application, which included the sensitivity analysis for the water intrusion behavior. For this study, a dry gas model was used with field production data in the base case. This model used a grid measuring (47, 41, 4) in the (x, y, z) axes, respectively. The model contained 12,253 natural fractures in each of the sensitivity scenarios. There were 5 wells in the model: 4 horizontal and 1 vertical well. Their respective lengths and trajectories are below in *Table 10*.

Well	Orientation	Lateral Length (m)
B1	Horizontal	337
B3	Horizontal	471.4
B4	Horizontal	351.8
B5	Horizontal	653.2
B2	Vertical	N/A

Table 10: Wells included in the field study with their associated orientation and lateral length, if applicable.

Each well's positioning within the grid is shown with the grid in *Figure 56*.

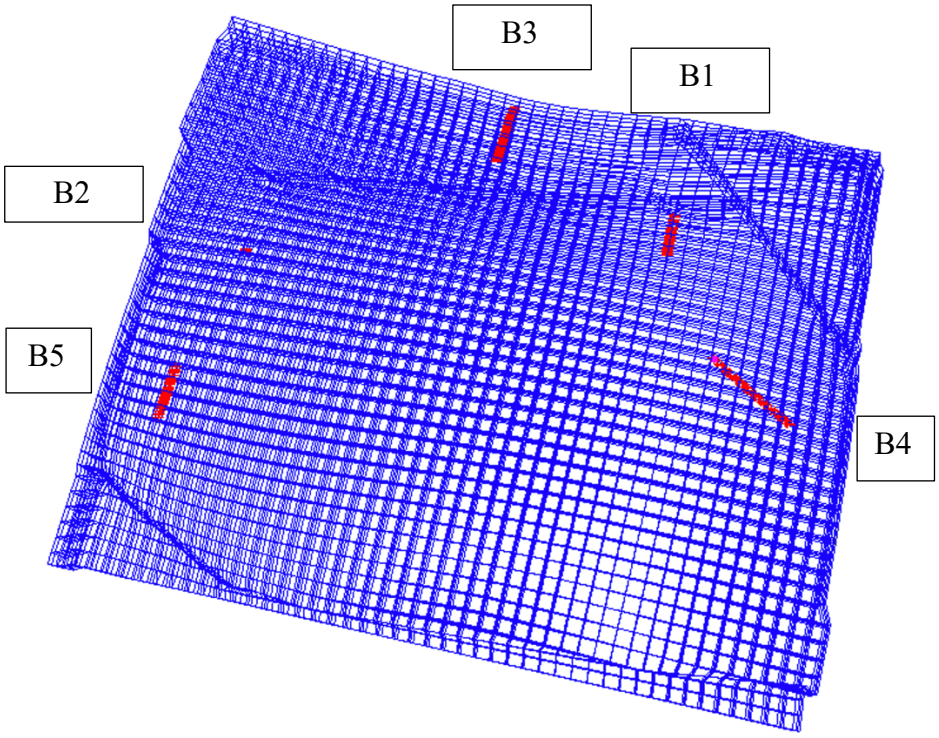

Figure 56: Visualization of the grid, wells, and their positioning for the field study.

3.2 GRID MODEL

The matrix properties for the model are found in Table 11.

Parameter	Value
Porosity, %	7
Permeability, mD	0.005
Kv/Kh	0.1
Initial Water Saturation	0.4385
Reservoir Pressure, kPa	58,470
Avg. Reservoir Thickness, m (z)	40

Table 11: Matrix properties for the field study.

Each well and its position within the model along with the grid's formulation are in Figure 57. From the model, there are a higher concentration of natural fractures in the upper portion of the model. Additionally, the wells were brought on at different times. The timing of their initial production can be found in Table 12.

Well	Initial Prod. Compared to 101D
B1	0 Months
B2	0 Months
B3	2.5 Months
B4	19.7 Months
B5	11.5 Months

Table 12: Wells and their initial production with respect to the original wells (B1 and B2) coming online.

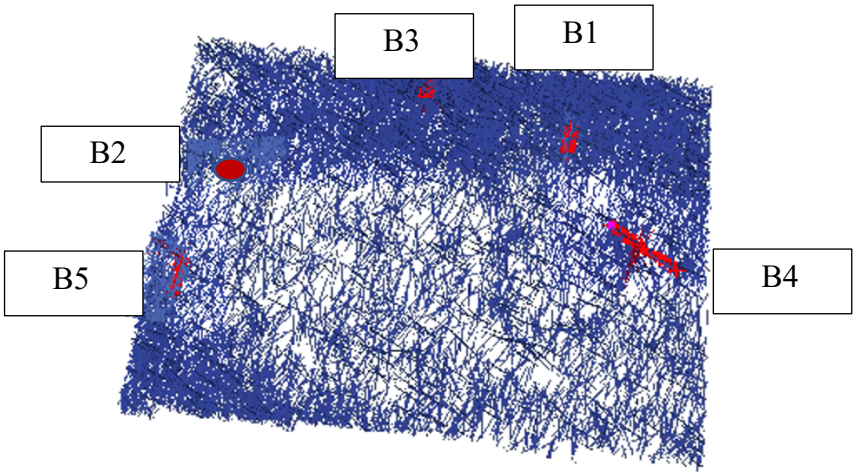

Figure 57: Visualization of the fracture model with the associated wells and fractures.

3.3 Sensitivities

Similar to the conceptual model, sensitivities were run on these natural fractures in order to determine the effect of varying natural fracture properties on gas production and

water production. Because this is a field case, the production was compared to the reported production history instead of a base case scenario, as in the conceptual model. Due to the lag in the production for some of the wells, and with the hope of avoiding depletion effects and interaction between parent and child wells, 101D was chosen as the well of interest for this sensitivity study. The variables used in the sensitivity study were natural fracture conductivity, natural fracture length, aquifer thickness, and aquifer permeability. These variables and their low and high ranges are given in Table 13. It should be noted that the base case contained ranges of these variables, but their average value is included in Table 13.

Natural Fracture Property	**Low Value**	**High Value**	**Base (avg)**
Conductivity (mD-m)	1	1000	66
Number of Natural Fractures	3541	12,253	12,253
Aquifer Thickness (m)	20	80	40
Aquifer Permeability (mD)	0.1	10	1

Table 13: Sensitivity variables with their low and high value as compared to the average base value in this field study.

In the *Table 13*, the reason the base case does not have average aquifer thickness or aquifer permeability is because the original field study did not include the presence of an aquifer. For this sensitivity study the Fetkovich aquifer and its formulation were used. It should be noted, that one difference between the field study and the conceptual model is the simplifying assumption of the fracture geometries. In the conceptual model, planar fractures – which use to points (x_1, y_1, z_1) and (x_2, y_2, z_2) to model the fracture – were used. For the field study, polygons were used to model the fractures, which use 4 points - (x_1, y_1, z_1), (x_2, y_2, z_2), (x_3, y_3, z_3), and (x_4, y_4, z_4) – to create each fracture. This

modeling technique allows for more complex orientations and geometries in the fracture network. The sensitivities that were calculated were based on the inputs in *Table 13*.

3.4 RESULTS

The plots of the sensitivity study for natural fracture conductivity are below, in *Figures 58-61*. There is a slight disconnect between the sensitivities (0.1 md-m to 1000 md-m) in early time. However, there is almost no difference between the sensitivity curves, even over 4 orders of magnitude. This gives evidence that there is little influence on water rate, gas rate, or, in turn, water-gas ratio. This was hypothesized in the conceptual model, as the lowest sensitivity in all the studies was the natural fracture conductivity. It has been confirmed in this field case that the natural fracture conductivity does not drastically affect the water rate, gas rate, or water gas ratio compared to the number of natural fractures. There were slight increases in the water rate and water-gas ratio in Chapter 2's conceptual model. Additionally, there is evidence of a decrease in gas rate as the natural fracture conductivity increases. This is due to more water intrusion into these fractures, cutting off some of the flow of gas. Due to the large number of fractures, and their interactions in this grid, the conductivity had little effect, because the flow is governed by the number and length of the fractures in the grid.

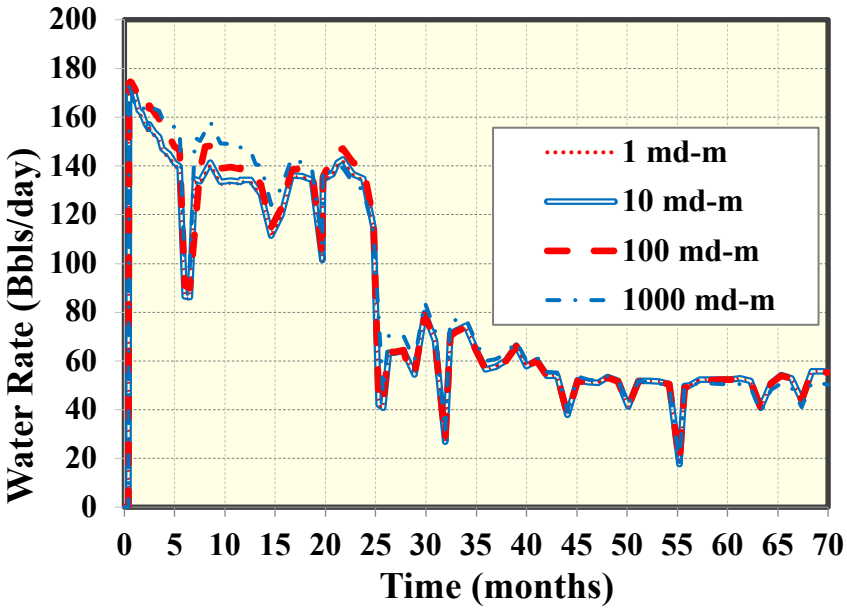

Figure 58: Water rate while varying the natural fracture conductivity and holding all other variables constant.

However conductive the fractures are, over a long period of time, did not drastically affect the water production because of the large number of fractures on the grid. This theory can be explained through the same reasoning as in Chapter 2. Natural fracture conductivity just increases the ability for fluid to travel through any given fracture. This is evident through the increased rates at early times for the higher conductivity natural fractures. It does not increase the surface area of these fractures and can, potentially, leave some fractures isolated. Like a highway system, this increased conductivity just increases the speed at which the cars can travel down the road. The increased surface area, in theory, widens the highway, allowing for higher of volumes of traffic to travel down. The increased interconnectivity gives more roads, or pathways, to the fluid's destination – the wellbore. This theory was further confirmed with the sensitivity study on the number of natural fractures within the field study model.

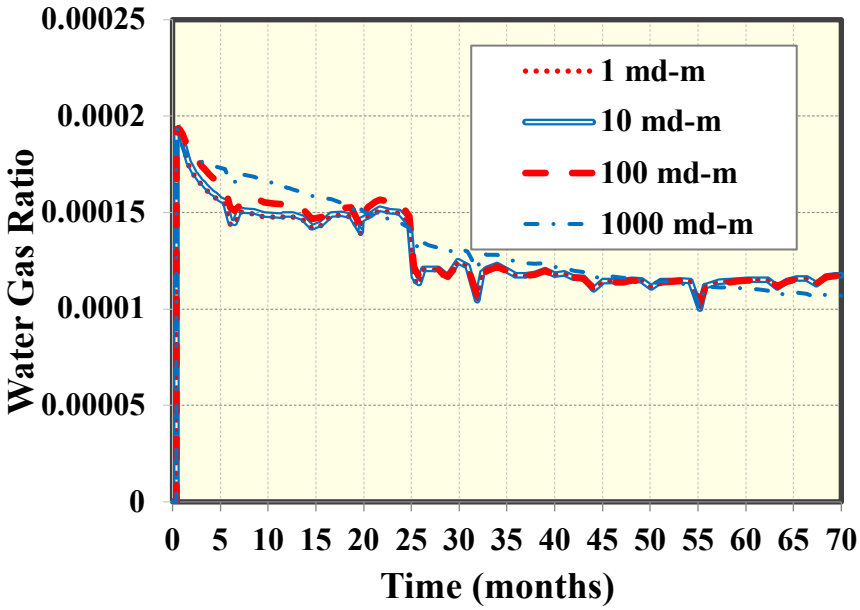

Figure 59: Water-Gas Ratio varying natural fracture conductivity and holding all other variables constant.

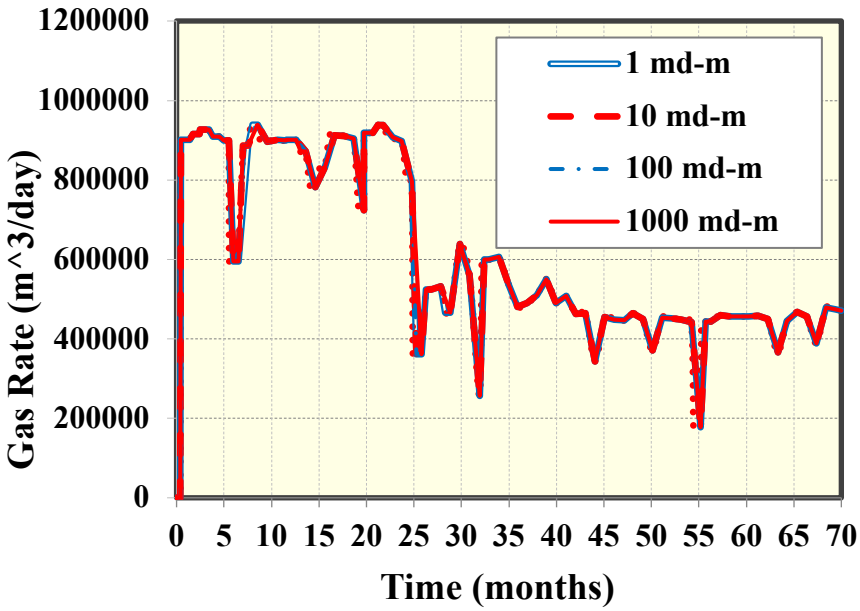

Figure 60: Gas rate varying natural fracture conductivity and holding all other variables constant.

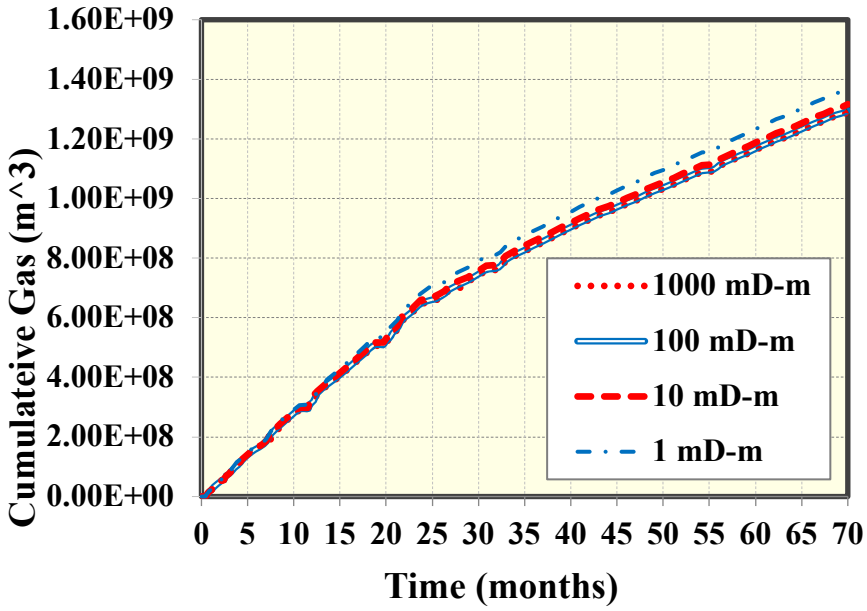

Figure 61: Cumulative gas production (m^3) for varying natural fracture conductivities for the field study.

Figures 62-65, plots of the water rate, gas rate, and water-gas ratio are displayed while varying natural fracture number in the reservoir. The values of the number of fractures, in this study, were 3541, 6041, and 12,253. The plots show a slight increase in water rate, and water gas-ratio at increasing natural fracture amounts. They also show a slight decrease in peak gas rate as the number of natural fractures decreases and an increase in cumulative oil as the number of natural fractures increases. These peaks then converge in the later producing months (24 months and on). These results are consistent with the results of the conceptual model.

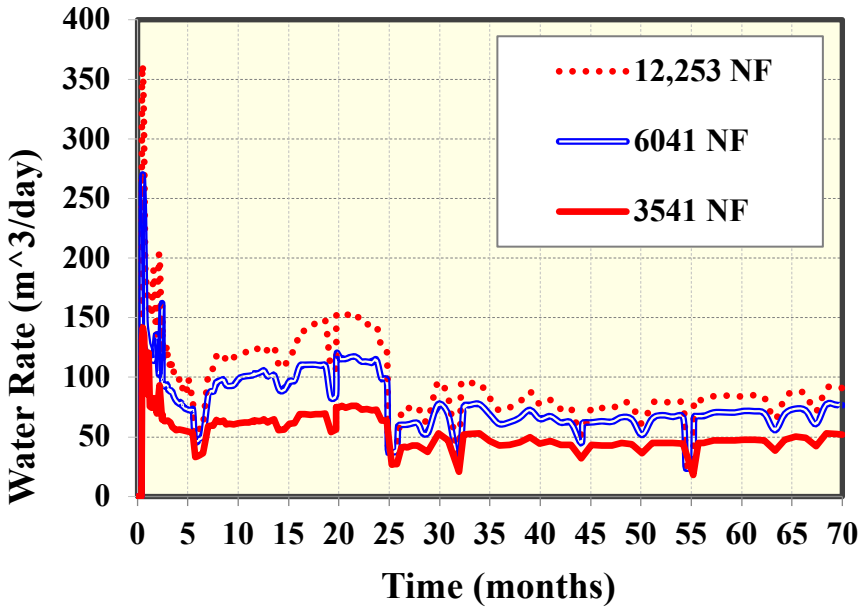

Figure 62: Water rate at varying numbers of natural fractures in the reservoir model.

These results are a consequence of the Fetkovich aquifer beneath the reservoir. As gas and initial water saturations are produced, water from the aquifer fills the depleted reservoir rock. Over time, this process increases the producing water rate as more water is able to intrude into those fractures. This results in higher early-time gas production, that decreases as the water intrudes into the natural fracture networks.

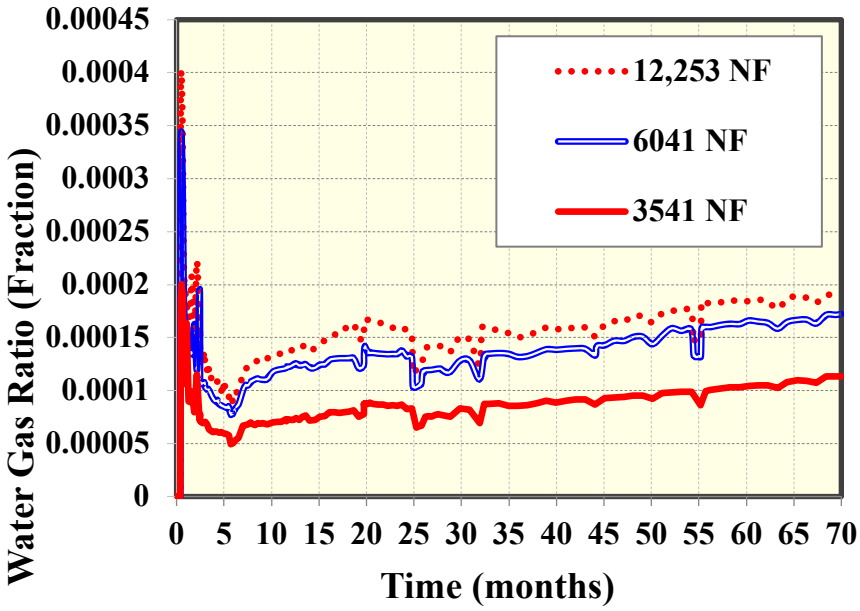

Figure 63: Water-gas ratio at varying numbers of natural fractures in the reservoir model.

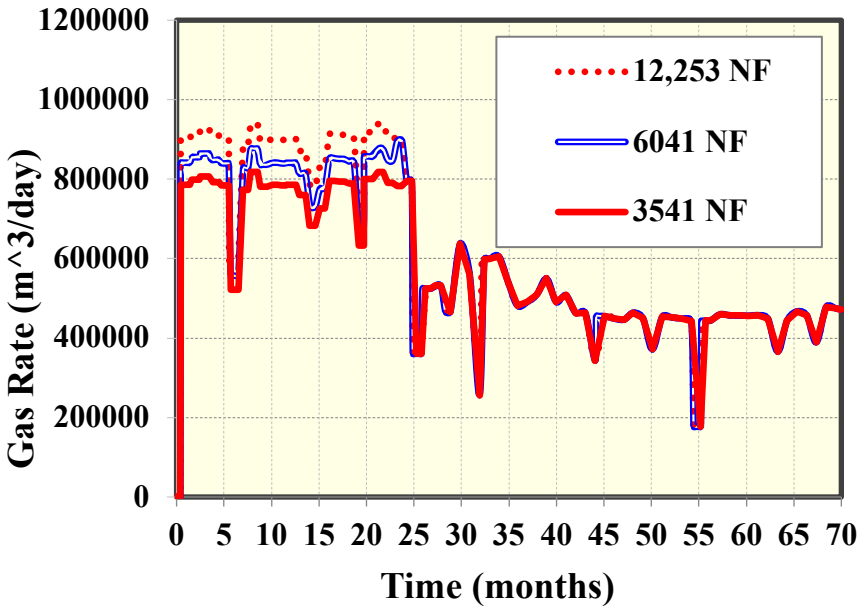

Figure 64: Gas rate at varying numbers of natural fractures in the reservoir model.

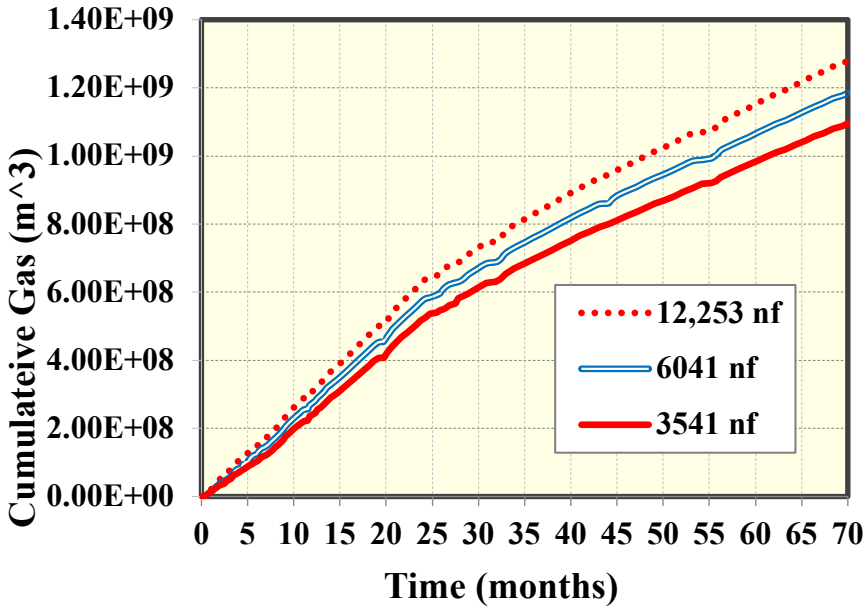

Figure 65: Cumulative gas rate at varying number of natural fractures for the field study case.

The final sensitivity analysis was done by varying the aquifer thickness and aquifer permeability for a Fetkovich aquifer connected on the bottom of the reservoir. The aquifer thickness did not have any true effect on the water rate, gas rate, or water-gas ratio. Their plots are below in *Figures 66-67*. These plots just show the water rate for the increasing aquifer thickness and increasing aquifer permeability. The aquifer permeability does have an effect on the water rate. As aquifer permeability increases the water rate increases as well. These results can be explained by the semi-infinite nature of the aquifer in this model. Since there is an almost infinite water supply beneath the reservoir, an increased permeability of the aquifer would increase the amount of water produced by the wellbore. The strong aquifer is able to, more easily, intrude into the reservoir and natural fracture networks with a higher permeability value. This effect, while not readily evident in the water rate plot, was evident in the cumulative gas plots and sensitivities.

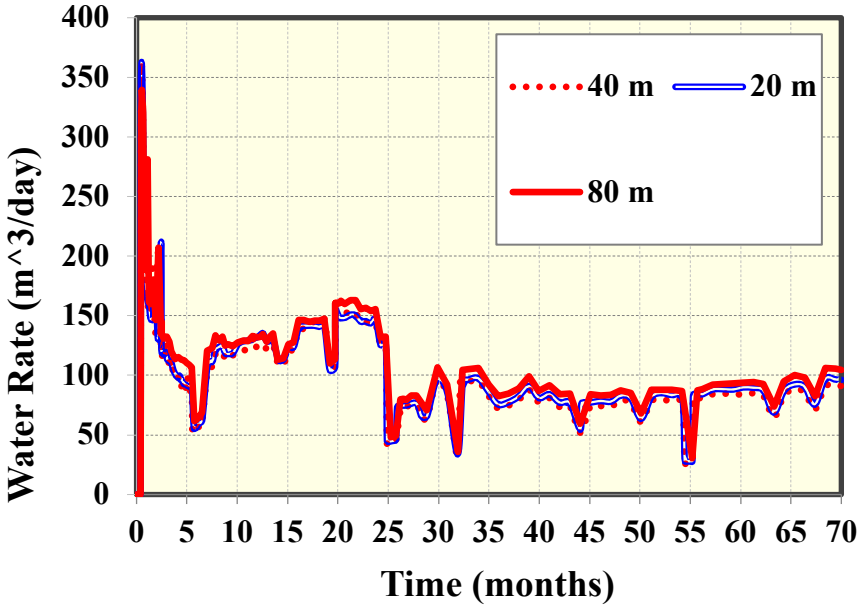

Figure 66: Water rate at varying aquifer thicknesses.

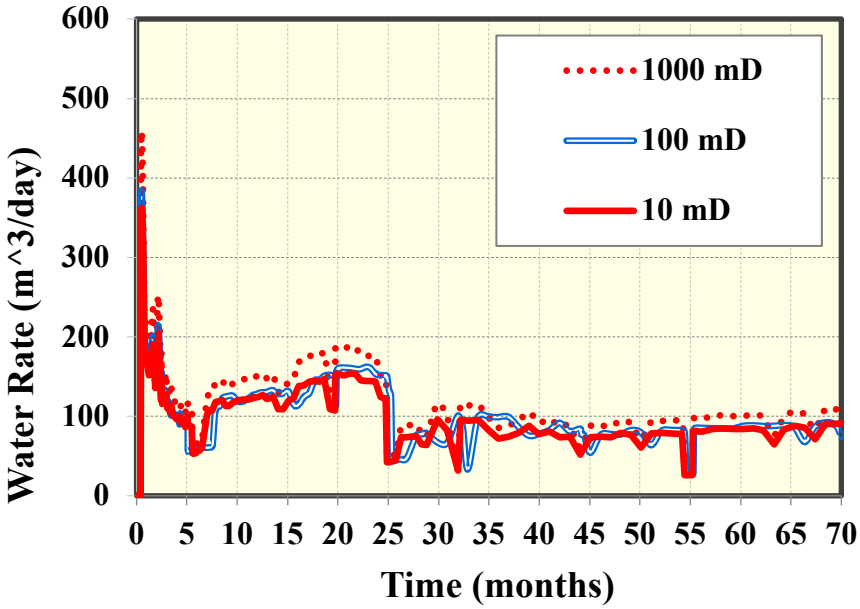

Figure 67: Water rate at varying aquifer permeability.

Figures 68-69 show the natural fracture pressure depletion and natural fracture water saturations at the final time step. It should be noted the original reservoir pressure was 58,470 kPa and the initial water saturation in the reservoir was 0.4385. There is evidence of lower natural fracture pressure and higher natural fracture water saturations near the wells. The higher water saturation is due to the intrusion of water from the reservoir. The lower pressure in the fractures is due to their initial depletion of hydrocarbons and initial water saturation that has now been filled by the aquifer intrusion.

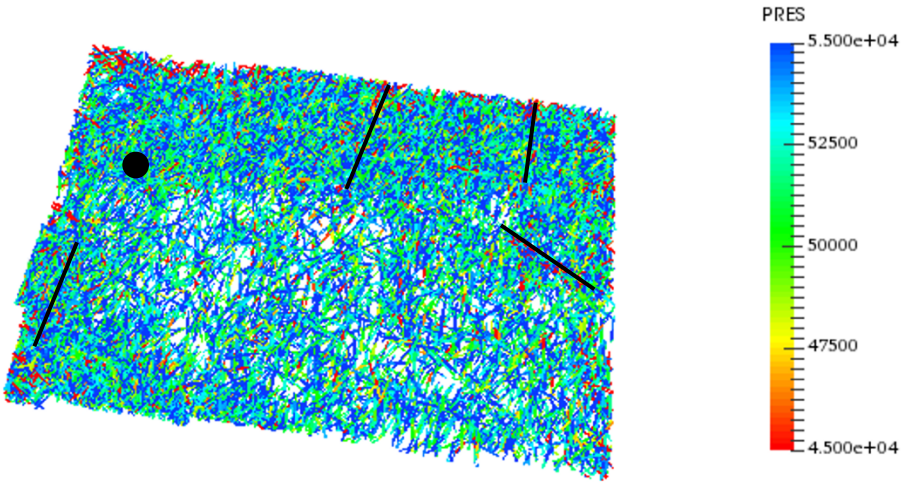

Figure 68: Natural fracture pressure for the base case at the final time step (70 months of production). Pressure is in kPa.

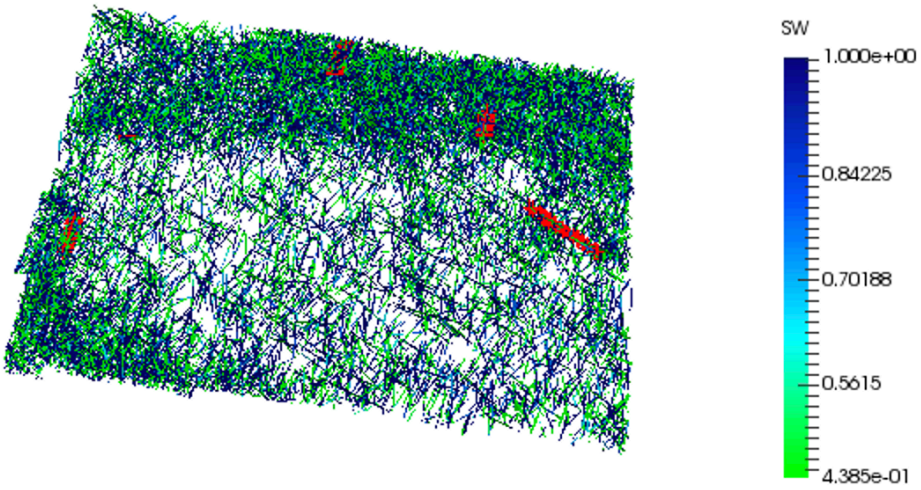

Figure 69: Natural fracture water saturation of the base case at the final time step (70 months of production).

Figure 70 show the initial pressure distribution in the grid at t=0. *Figure 71* displays the final pressure distribution after 70 months of production.

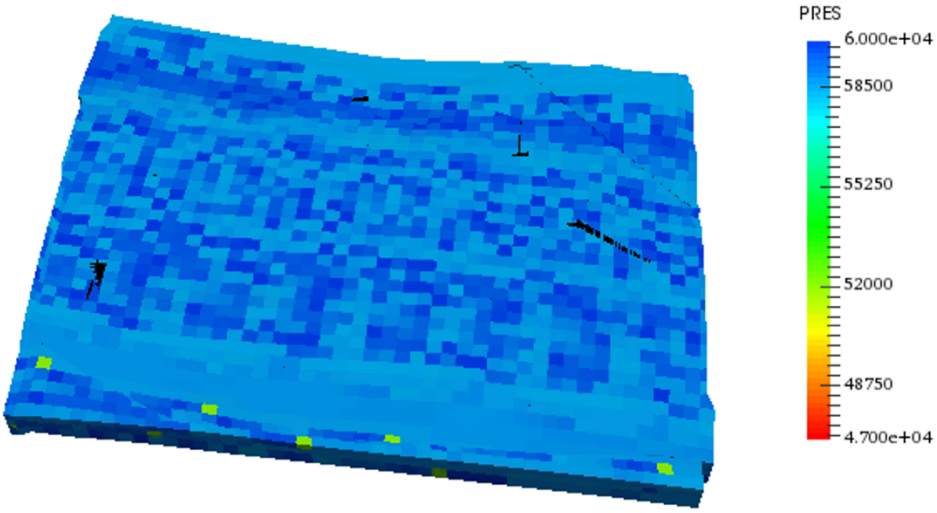

Figure 70: Initial pressure distribution for the field study at t=0 months.

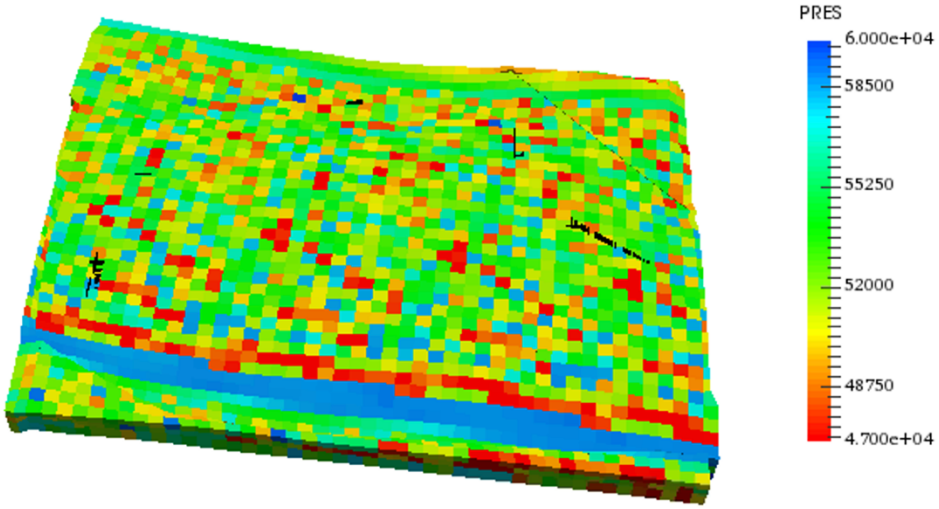

Figure 71: Final pressure distribution at t=70 months of production for the field study.

3.5 Sensitivity Analysis

Below are the sensitivity plots, in *Figures 72-75*, formatted as tornado diagrams for the field study. These plots differ from the conceptual model because the aquifer permeability, and fracture number were related to the base case, which occurred at maximum fracture number and minimum aquifer permeability. It is still clear that, as you decrease fracture number – from the maximum of 12,253 – the water rate, peak gas rate, and water gas ratio decrease. As you increase the aquifer permeability, from the base case of 10 mD, water rate and water-gas ratio increase.

It is clear from these plots that the primary sensitivity is to the number of natural fractures (labeled “Density on the plot) within the grid. Secondary to that is the aquifer permeability, however the aquifer permeability has very little effect on the peak gas rate. This is due to the peak gas rate happening at an early time, before the aquifer has had sufficient time to intrude and reduce the gas rate. Natural fracture conductivity was the

least sensitive variable in this study. This is due to the importance and governance of flow through the fracture networks. These networks are cut short, and fractures isolated when the number of natural fractures is decreased. Therefore, the number of natural fractures had a higher effect on water rate, peak gas rate, cumulative gas produced and water-gas ratio.

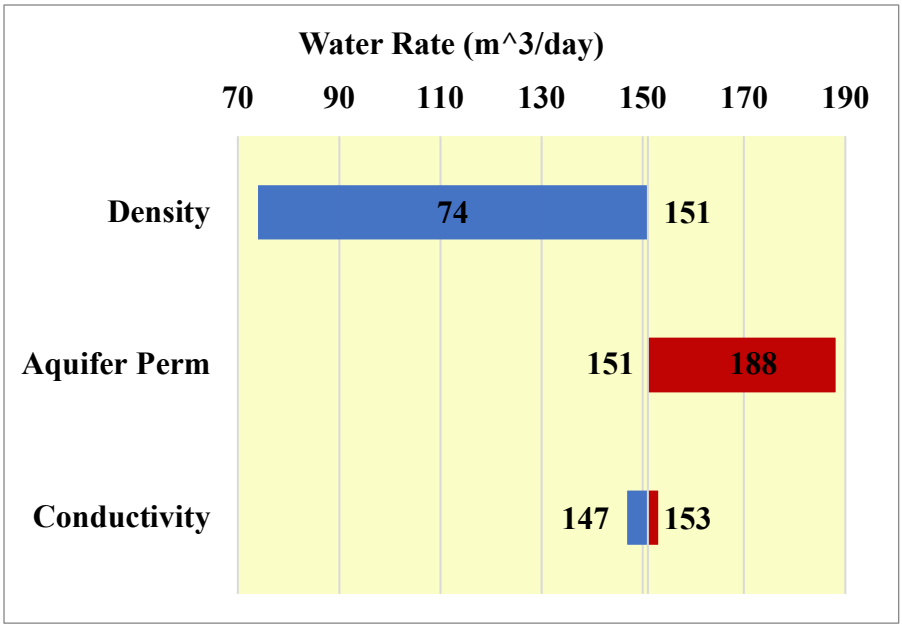

Figure 72: Sensitivity plot of the effect on water rate while varying natural fracture density, aquifer permeability and natural fracture conductivity

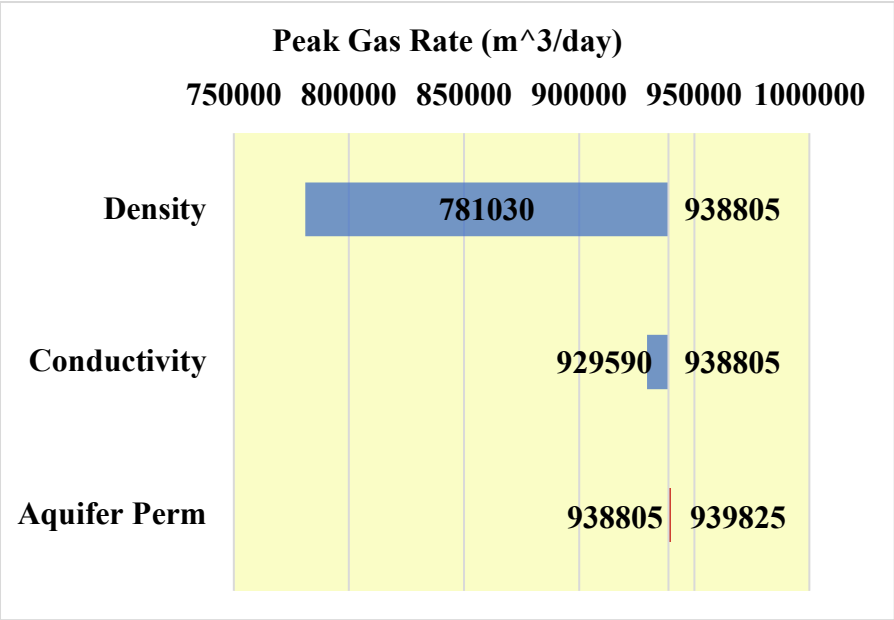

Figure 73: Sensitivity plot of the effect on peak gas rate while varying natural fracture density, aquifer permeability and natural fracture conductivity.

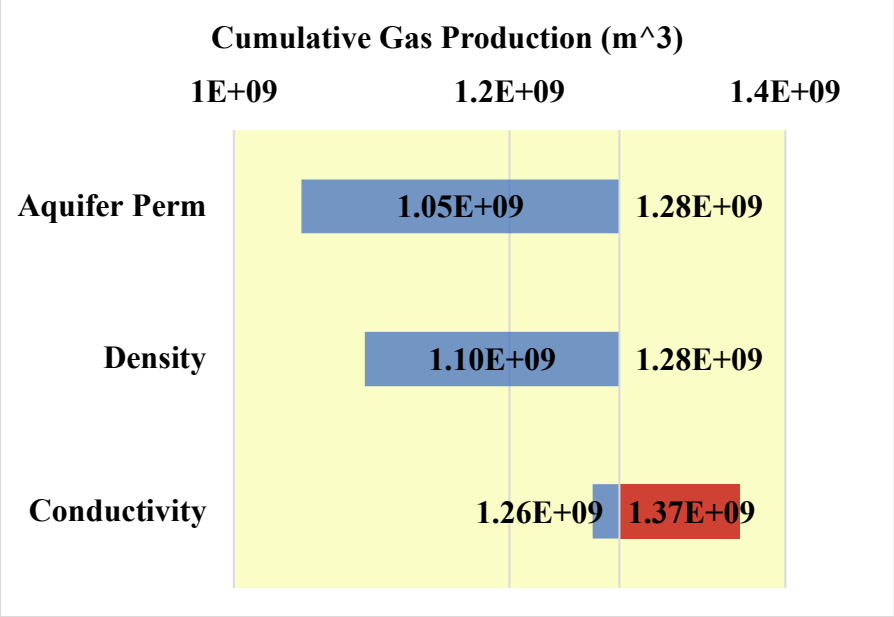

Figure 74: Sensitivity plot of the effect on Cumulative Gas Production of varying aquifer permeability, number of natural fractures and natural fracture conductivity.

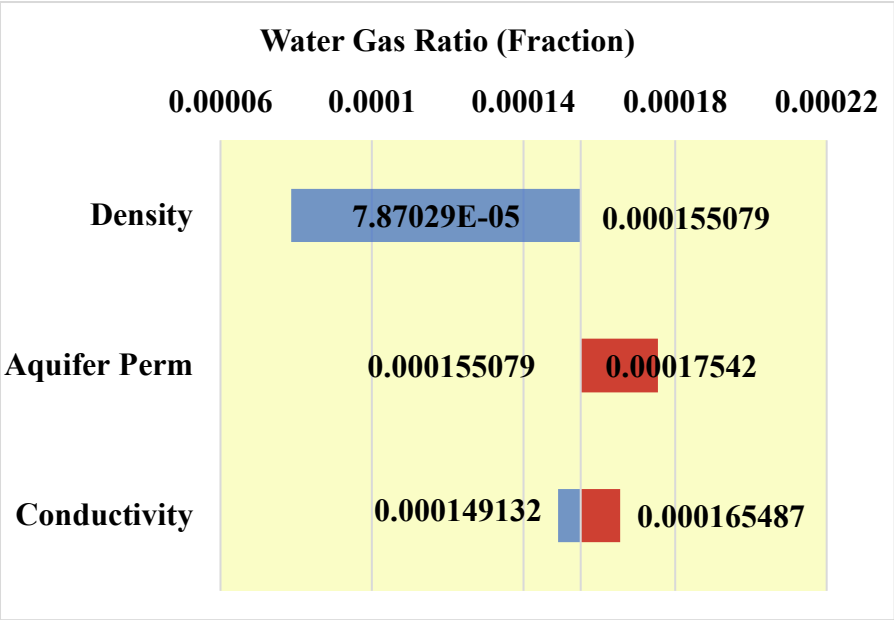

Figure 75: Sensitivity plot of the effect on water-gas ratio while varying natural fracture density, aquifer permeability and natural fracture conductivity

Chapter 4: Conclusions

From the conceptual model we learned about the effect natural fracture properties (conductivity, density, and number of fractures) has on the production of fluids and water intrusion into the wellbore. The tight reservoir model showed that increasing the number of natural fractures and the conductivity (aperture and permeability) increased the amount of fluid produced. There were higher production rates of water, and higher gas and oil cumulative productions at increasing natural fracture number and conductivity. Additionally, the most sensitive variable in the tight reservoir model was the number of natural fractures on the grid. This is due to the increased surface area and conductivity in the reservoir volume. By adding more natural fractures, it reduces the number of isolated and allows the fluid to flow more quickly through the fracture network to the wellbore. Flow is governed by natural and hydraulic fractures in tight reservoirs.

In the carbonate model, the aquifer was added to determine how its presence affects the understanding developed in the tight reservoir model. A similar trend showed, but the presence of the aquifer, in many cases, decreased the gas rate, and cumulative gas production. This is due to intrusion of the aquifer into the highly conductive fracture networks. The results and sensitivity analysis showed that increasing the surface area, and interconnectivity of these fractures (increasing number of fractures, or lengths of fractures) increased the peak gas rate and cumulative gas rate, but also increased the likelihood of natural fracture interaction with the aquifer. In cases where there was evidence of natural fracture interaction with the aquifer, gas production decreased after some time, while water rate increased. Sensitivity analysis showed that the most sensitive variables in the study were the number of natural fracture and natural fracture length.

In the field study, the trends from Chapter 2 were confirmed and built upon. Decreasing the number of natural fractures, decreased the peak gas rate and the water rate. This shows that decreasing the surface area and interconnectivity of natural fractures reduces the fluid production. Additionally, the field case showed that varying the aquifer permeability allows for more water intrusion into the reservoir and increases the water rate for higher aquifer permeabilities. The fluid production rates and cumulative productions were most sensitive to the number of natural fractures present in the model.

For the study as a whole, adding more fractures, to a fixed volume, creates more highly conductive pathways for the fluid to flow through. Additionally, as more fractures are added, even at random, they have a higher probability of interacting with each other and creating a faster flow path to the wellbore. When an aquifer is present, due to the strength of the aquifer, as pressure decreases in the reservoir water invades these fractures and saturates them, further influencing more water flow to the wellbore. This explains the increase in the water producing rates, water ratios, and the potential for decline in gas rates and cumulative gas production over time with an increasing number and length of natural fractures.

Glossary

ACRONYMS

BBLs	=	Barrels of Oil
DFM	=	Discrete Fracture Modeling
EDFM	=	Embedded Discrete-Fracture Modeling
GOR	=	Gas-Oil Ratio
LGR	=	Local Grid Refinement
mD	=	Milli-Darcy
nf	=	Natural Fractures
NNC	=	Non-Neighboring Connections

NOMENCLATURE

A_{NNC}	=	Contact area
b	=	Width in ft
B_1	=	Constant of proportionality defined by flow regime, geologic properties
c_e	=	Composite compressibility of the oil reservoir
c_t	=	Total or effective aquifer compressibility
d_f	=	Average of normal distances from center of the fracture to intersection
d^{NNC}	=	Distance of natural fracture
dv	=	Volume element
h	=	Height in ft
k	=	Aquifer permeability
k_f	=	Fracture permeability
k^{NNC}	=	Non-neighboring connection permeabilty
L	=	Length in ft
L_{int}	=	Length of the intersection line
n_{NNC}	=	Number of non-neighboring connections
P	=	Function defined at t_{Dj}
P'	=	Derivative of the function P
Δp	=	The change in pressure from $p(0) - \mathrm{p}(t_{D_j})$
$\bar{p}$	=	Average aquifer pressure
p_{wf}	=	Inner aquifer boundary pressure
$P_j - \gamma_j D$	=	Potential variation between neighboring cells
q_i^{NNC}	=	Molar flow rate of component i
q_w	=	Water flow rate

r_a = External radius of the aquifer
r_r = Internal radius of the aquifer
t = Time, days
t_{D_j} = Present time step
$t_{D_{j-1}}$ = The previous time step
V = Volume of grid block
W_e = Cumulative water influx at current time-step
x_n = Normal distance
μ = Viscosity of the fluid
ϕ = Porosity
ω_f = Fracture Aperture

References

Barenblast, G.I., & Zheltov, Y.P. (1960). *Fundamental Equations of Filtration of Homogeneous Liquids in Fissured Rocks*. Soviet Physics-Doklady, Vol. 5.

Beattie, D. R., & Roberts, B. E. (1996, January 1). Water Coning in Naturally Fractured Gas Reservoirs. Society of Petroleum Engineers. Paper SPE-35643-MS, presented at SPE Gas Technology Symposium, Calgary, Alberta, Canada, 28 April-1 May.

Burrows, Lauren & Haeri, Foad & Cvetic, Patricia & Sanguinito, Sean & Shi, Fan & Tapriyal, Deepak & Goodman, Angela & Enick, Robert. (2020). A Literature Review of CO 2 , Natural Gas, and Water-Based Fluids for Enhanced Oil Recovery in Unconventional Reservoirs. *Energy & Fuels* **34**(5), 5331-5380.

Carter, R. D., & Tracy, G. W. (1960, December 1). An Improved Method for Calculating Water Influx. *Transactions of AIME* **219**(1), 415-417.

Cavalcante Filho, J. S. De Araujo, Shakiba, M., Moinfar, A., & Sepehrnoori, K. (2015, February 23). Implementation of a Preprocessor for Embedded Discrete Fracture Modeling in an IMPEC Compositional Reservoir Simulator. Paper SPE-173289-MS, presented at the SPE Reservoir Simulation Symposium, Houston, Texas, 23-25 February.

Chen P, Fiallos-Torres M, Xing Y, Yu W, Guo C, Leines-Artieda J, Cheng M, Xie H, Shi H, Mao Z, Miao J, Sepehrnoori K. (2020). Water Intrusion Characterization in Naturally Fractured Gas Reservoir Based on Spatial DFN Connectivity Analysis. *Energies* **13**(16), 4235

Cipolla, C. L., Warpinski, N. R., Mayerhofer, M., Lolon, E. P., & Vincent, M. (2010, November 1). The Relationship Between Fracture Complexity, Reservoir Properties, and Fracture-Treatment Design. Paper SPE-115769-MS, presented at SPE Annual Technical Conference and Exhibition, Denver, Colorado, 21-24 September.

De Swaan O., A. (1976, June 1). Analytic Solutions for Determining Naturally Fractured Reservoir Properties by Well Testing. *Society of Petroleum Engineers Journal* **16**(03), 117-122.

Dean, R. H., & Lo, L. L. (1988, May 1). Simulations of Naturally Fractured Reservoirs. *SPE Reservoir Engineering* **3**(02), 638-648.

Fetkovich, M. J. (1971, July 1). A Simplified Approach to Water Influx Calculations-Finite Aquifer Systems. *Journal of Petroleum Technology* **23**(07), 814-828.

Fisher, M. K., Heinze, J. R., Harris, C. D., Davidson, B. M., Wright, C. A., & Dunn, K. P. (2004, January 1). Optimizing Horizontal Completion Techniques in the Barnett Shale Using Microseismic Fracture Mapping. Paper SPE-90051-MS, presented at SPE Annual Technical Conference and Exhibition, Houston, Texas, 26-29 September.

Gale, Julia & Reed, Robert & Holder, Jon. (2007). Natural fractures in the Barnett Shale and their importance for hydraulic fracture treatments. *AAPG* **91**(4), 603-622.

Hajibeygi, Hadi & Karvounis, Dimitrios & Jenny, Patrick. (2011). A Hierarchical Fracture Model for the Iterative Multiscale Finite Volume Method. *Journal of Computational Physics* **230**(24), 8729-8743.

Hoteit, H., & Firoozabadi, A. (2006, September 1). Compositional Modeling of Discrete-Fractured Media Without Transfer Functions by the Discontinuous Galerkin and Mixed Methods. *SPE Journal* **11**(3), 341-352.

Hui, M.-H., Mallison, B. T., Fyrozjaee, M. H., & Narr, W. (2013, September 30). The Upscaling of Discrete Fracture Models for Faster, Coarse-Scale Simulations of IOR and EOR Processes for Fractured Reservoirs. Paper SPE-166075-MS, presented at SPE Annual Technical Conference and Exhibition, New Orleans, Louisiana, 30 September-2 October.

Hurst, W. (1958, December 1). The Simplification of the Material Balance Formulas by the Laplace Transformation. *Transactions of AIME* **213**(1), 292-303.

Inikori, Solomon. (2002). Numerical Study of Water Coning Control with Downhole Water Sink (DWS) Completions in Vertical and Horizontal Wells. *LSU Doctorial Dissertations*. 2287.

Izgec, B., & Barrufet, M. A. (2005, January 1). Performance Analysis of Compositional and Modified Black-Oil Models for a Rich Gas Condensate Reservoir. Paper SPE-93374-MS, presented at SPE Western Regional Meeting, Irvine, California, 30 March-1 April.

Karimi-Fard, Mohammad & Firoozabadi, Abbas. (2003). Numerical Simulation of Water Injection in Fractured Media Using the Discrete-Fracture Model and the Galerkin Method. *SPE Reservoir Evaluation and Engineering* **6**(2), 117-126.

Karimi-Fard, M., Durlofsky, L. J., & Aziz, K. (2004, June 1). An Efficient Discrete-Fracture Model Applicable for General-Purpose Reservoir Simulators. *SPE Journal* **9**(2), 227-236.

Lee, S. & Lough, M. & Jensen, C. (2001). Hierarchical Modeling of Flow in Naturally Fractured Formations with Multiple Length Scales. Water Resources Research **37**(3), 443-455.

Li, L., & Lee, S. H. (2008, August 1). Efficient Field-Scale Simulation of Black Oil in a Naturally Fractured Reservoir Through Discrete Fracture Networks and Homogenized Media. *SPE Reservoir Evaluation & Engineering* **11**(4), 750-758.

Loucks, Robert G., Reed, Robert M., Ruppel, Stephen C., Hammes, Ursula (2012). Spectrum of pore types and networks in mudrocks and a descriptive classification for matrix-related mudrock pores. *AAPG Bulletin* **96**(6), 1071–1098.

Matthai, Stephan & Mezentsev, A. & Belayneh, M. (2005). Control-Volume Finite-Element Two-Phase Flow Experiments with Fractured Rock Represented by Unstructured 3D Hybrid Meshes. Paper SPE-93341-MS, presented at SPE Reservoir Simulation Symposium, The Woodlands, Texas, 31 January-2 February.

Maxwell, S. C., Urbancic, T. I., Steinsberger, N., & Zinno, R. (2002, January 1). Microseismic Imaging of Hydraulic Fracture Complexity in the Barnett Shale. Paper SPE-77440-MS, presented at SPE Annual Technical Conference and Exhibition, San Antonio, Texas, 29 September-2 October.

Moinfar, A., Varavei, A., Sepehrnoori, K., & Johns, R. T. (2014, April 1). Development of an Efficient Embedded Discrete Fracture Model for 3D Compositional Reservoir Simulation in Fractured Reservoirs. *SPE Journal* **19**(2), 289-303.

Monteagudo, Palomino, Jorge & Firoozabadi, Abbas. (2004). Control-volume Method for Numerical Simulation of Two-Phase Immiscible Flow in Two- and Three-Dimensional Discrete-Fractured Media. *Water Resources Research* **40**(7). W07405.

Noorishad, J., & Mehran, M. (1982). An Upstream Finite Element Method for Solution of Transient Transport Equation in Fractured Porous Media. *Water Resources Research* **18**(3), 588-596.

Panfili, P., & Cominelli, A. (2014, November 10). Simulation of Miscible Gas Injection in a Fractured Carbonate Reservoir using an Embedded Discrete Fracture Model. Paper SPE-171830-MS, presented at Abu Dhabi International Petroleum Exhibition and Conference, Abu Dhabi, UAE, 10-13 November.

Sandve, Tor Harald & Berre, Inga & Nordbotten, J.M.. (2012). An Efficient Multi-Point Flux Approximation Method for Discrete Fracture–Matrix Simulations. *Journal of Computational Physics* **231**(9), 3784–3800.

Shen, Weijun & Liu, Xiao-hua & Li, Xi-zhe & Lu, Jialiang. (2015). Water Coning Mechanism in Tarim Fractured Sandstone Gas Reservoirs. *Journal of Central South University* **22**(1), 344-349.

Syed-Kechik, M. B., & Hutchinson, H. L. (1983, January 1). Numerical Simulation of Aquifers Using Transient Grid Block Properties. Paper SPE-12156-MS, presented at SPE Annual Technical Conference and Exhibition, San Francisco, California, 5-8 October.

Van Everdingen, A.F. and Hurst, W. (1949) The Application of the Laplace Transformation to Flow Problems in Reservoirs. *Journal of Petroleum Technology* **1**(12), 305-324.

Warpinski, N. R., Mayerhofer, M. J., Vincent, M. C., Cipolla, C. L., & Lolon, E. P. (2008). Stimulating Unconventional Reservoirs: Maximizing Network Growth While Optimizing Fracture Conductivity. Paper SPE-114173-MS, presented at SPE Unconventional Reservoirs Conference, Keystone, Colorado, 10-12 February.

Xu, Y., Cavalcante Filho, J. S. A., Yu, W., & Sepehrnoori, K. (2017, May 1). Discrete-Fracture Modeling of Complex Hydraulic-Fracture Geometries in Reservoir Simulators. *SPE Reservoir Evaluation and Engineering* **20**(02), 403-422.

Xu, Y., Yu, W., & Sepehrnoori, K. (2017, July 24). Modeling Dynamic Behaviors of Complex Fractures in Conventional Reservoir Simulators. Paper URTEC-2670513-MS, presented at SPE/AAPG/SEG Unconventional Resources Technology Conference, Austin, Texas, 24-26 July.